

# UV-extended E-MILES stellar population models: young components in massive early-type galaxies

A. Vazdekis<sup>1,2\*</sup>, M. Koleva<sup>3</sup>, E. Ricciardelli<sup>4</sup>, B. Röck<sup>1,2</sup>, J. Falcón-Barroso<sup>1,2</sup>

<sup>1</sup>*Instituto de Astrofísica de Canarias (IAC), E-38200 La Laguna, Tenerife, Spain*

<sup>2</sup>*Departamento de Astrofísica, Universidad de La Laguna, E-38205, Tenerife, Spain*

<sup>3</sup>*Sterrenkundig Observatorium, Ghent University, Krijgslaan 281, S9, B-9000 Ghent, Belgium*

<sup>4</sup>*Laboratoire d'astrophysique, École Polytechnique Fédérale de Lausanne (EPFL), Observatoire, 1290 Versoix, Switzerland*

Published: 2016MNRAS.463.3409V

## ABSTRACT

We present UV-extended E-MILES stellar population synthesis models covering the spectral range  $\lambda\lambda$  1680 – 50000 Å at moderately high resolution. We employ the NGSL space-based stellar library to compute spectra of single-age, single-metallicity stellar populations in the wavelength range from 1680 to 3540 Å. These models represent a significant improvement in resolution and age/metallicity coverage over previous studies based on earlier space-based libraries. These model spectra were joined with those we computed in the visible using MILES, and other empirical libraries for redder wavelengths. The models span the metallicity range  $-1.79 \leq [M/H] \leq +0.26$  and ages above 30 Myr, for a suite of IMF types with varying slopes. We focus on the behaviour of colours, spectra and line-strength indices in the UV range as a function of relevant stellar population parameters. Whereas some indices strengthen with increasing age and metallicity, as most metallicity indicators in the visible, other indices peak around 3 Gyr for metal-rich stellar populations, such as Mg at 2800 Å. Our models provide reasonably good fits to the integrated colours and most line-strengths of the stellar clusters of the Milky-Way and LMC. Our full-spectrum fits in the UV range for a representative set of ETGs of varying mass yield age and metallicity estimates in very good agreement with those obtained in the optical range. The comparison of UV colours and line-strengths of massive ETGs with our models reveals the presence of young stellar components, with ages in the range 0.1 – 0.5 Gyr and mass fractions 0.1 – 0.5%, on the top of an old stellar population.

**Key words:** galaxies: abundances – galaxies: elliptical and lenticular, cD – galaxies: stellar content – globular clusters: general

## 1 INTRODUCTION

The study of colours, line-strength indices and spectral energy distributions (SEDs) of unresolved star clusters and galaxies allows us to determine fundamental physical properties that are related to their stellar populations, such as the Star Formation History (SFH), age, metallicity, abundance element pattern, Initial Mass Function (IMF) and dust properties. Quantifying these properties is mandatory for an in-depth understanding of the formation and evolution of these systems. These studies are performed by comparing the observational data to predictions from stellar population synthesis models (e.g. Tinsley 1980). These models are also use-

ful for a wider community, such as, e.g., for kinematic studies, redshift measurements or constraining galaxy masses, just to mention some of the possible applications.

The so called evolutionary population synthesis models, which consider the relative contributions from all type of stars in the proportions prescribed by most recent advances in stellar evolution theory, are nowadays regarded as standard. Most of these models rely on three main ingredients, i.e. a prescription for the IMF, a set of stellar isochrones and stellar spectral libraries. The latter, which can either be theoretical or empirical, allow us to predict a variety of observables in several bands such as fluxes and colours, mass-to-light ratios (M/L), surface brightness fluctuations (SBFs), absorption line-strength indices or spectra with varying

\* E-mail: vazdekis@iac.es

resolutions. Such predictive abilities have made these models increasingly popular (e.g. Bressan, Chiosi & Fagotto 1994; Fritze-Von Alvensleben & Gerhard 1994; Worthey 1994; Vazdekis et al. 1996; Fioc & Rocca-Volmerange 1997; Kodama & Arimoto 1997; Maraston 1998; Leitherer et al. 1999; Bruzual & Charlot 2003; Schiavon 2007; Conroy & Gunn 2010; Chung et al. 2013).

Most detailed stellar population studies have focused so far on key absorption line indices, such as those of the Lick system (Worthey et al. 1994). By fitting these indices we are able to partially lift the main degeneracies affecting the colours, such as that between the age and the metallicity (e.g. Worthey 1994), and the abundances of various elements (e.g. Rose 1985; Thomas, Maraston & Bender 2003; Carretero et al. 2004; Yamada et al. 2006; Schiavon 2007; Conroy, Graves & van Dokkum 2014; Worthey, Baitian & Serven 2014), without being affected by dust (MacArthur 2005). This method has been mainly applied to early-type galaxies (ETGs) (e.g. Trager et al. 1998). With this type of analysis it has been possible to conclude that massive ETGs have mainly old stellar populations with the bulk of their stars formed at high redshift in very short timescales (e.g. Renzini 2006). A new generation of models predicting spectra of stellar populations at higher resolutions than is typically allowed by galaxy dynamics (as a result of the smearing due to their velocity dispersion), have opened new means to further improve these studies (e.g. Vazdekis 1999; Schiavon et al. 2002; Bruzual & Charlot 2003; Le Borgne et al. 2004; Vazdekis et al. 2010; Maraston & Strömbäck 2011; Conroy & van Dokkum 2012a). This has been possible by employing extensive empirical stellar spectral libraries, mostly in the optical range (e.g. Jones 1999; Prugniel & Soubiran 2001; Le Borgne et al. 2003; Valdes et al. 2004; Sánchez-Blázquez et al. 2006), but also theoretical libraries (e.g. Coelho et al. 2005). The latter has been employed for computing spectra of single-age, single-metallicity stellar populations (SSPs) with varying abundance ratios, either fully theoretical (e.g. Coelho et al. 2007) or combined with empirical libraries (e.g. Walcher et al. 2009; Vazdekis et al. 2015). These models provide greater abilities to define and optimize new line indices with enhanced sensitivities to relevant stellar population parameters (e.g. Serven, Worthey & Briley 2005; Cervantes & Vazdekis 2009), including IMF indicators (e.g. La Barbera et al. 2013; Spiniello et al. 2014), and full spectrum-fitting (e.g. Cid Fernandes et al. 2005; Ocvirk et al. 2006a; Koleva et al. 2009; Tojeiro et al. 2011).

Most of these detailed studies have been performed in the optical spectral range, despite the potential constraining power of the UV and Near-IR, which are dominated by different types of stars. There are models based on theoretical stellar libraries that provide us with low resolution SEDs redward the optical range (e.g., Bruzual & Charlot 2003; Maraston 2005; Conroy & Gunn 2010). It has been only recently that, by means of empirical stellar libraries (e.g. Cenarro et al. 2001a; Cushing, Raynier & Vacca 2005; Raynier, Cushing & Vacca 2009), we have at disposal SSP spectra at higher resolutions (e.g. Vazdekis et al. 2003; Conroy & van Dokkum 2012a; Meneses-Goytia et al. 2015; Röck et al. 2015).

The lack of libraries extending blueward  $\sim 3500 \text{ \AA}$

has prevented us to build models that allow us to perform detailed studies, such as those performed in the optical range. The UV spectral range is particularly sensitive to the hot components of galaxy stellar populations (e.g. Faber 1983). Therefore, the analysis of the UV places us in better position to properly characterise galaxy SFHs. Furthermore, as the various stellar population components contribute in different proportions to the different parts of the SED the combination of UV and optical (and/or Near-IR) data allows us to properly separate these contributions (e.g. Rose 1984; Schiavon, Caldwell & Rose 2004; Percival & Salaris 2011). The UV range is full of absorption features that are dominated by a variety of elements, which further inform us on the overall metallicity and individual abundance ratios (e.g. Fanelli et al. 1990; Davidge & Clark 1994; Ponder et al. 1998; Heap et al. 1998; Chavez et al. 2007; Maraston et al. 2009; Toloba et al. 2009; Serven et al. 2011). Blue Horizontal Branch (BHB) stars are claimed to be affecting the Far-UV range of globular clusters (e.g. de Boer 1985; Montes et al. 2014) or Extreme Horizontal Branch (EHB) stars as responsible for the UV-upturn phenomenon observed in a fraction of elliptical galaxies (e.g. Code & Welch 1979; Burstein et al. 1988; Dorman, O’Connell & Rood 1995; Kaviraj et al. 2007; Yi et al. 2011; Hernández-Pérez & Bruzual 2014). Very importantly, ground-based observing facilities allow us to obtain spectra of high redshift galaxies whose rest-frame UV fall in the optical or Near-IR spectral ranges, where the current instrumentation is most developed (e.g. Pettini et al. 2000; de Mello et al. 2004; Cimatti et al. 2005; Daddi et al. 2005; Mignoli et al. 2005; Popesso et al. 2009; van Dokkum & Brammer 2010).

A first attempt to obtain an empirical UV library with a reasonably large range of stellar parameters was observed by Wu et al. (1983) and Fanelli et al. (1992) with the International Ultraviolet Explorer<sup>1</sup> (IUE). This library is composed of 218 stars at resolution  $\sim 7 \text{ \AA}$  (FWHM), and it has been employed by the models of Bruzual & Charlot (2003) and Maraston et al. (2009). One of the shortcomings of the IUE is that the coverage in metallicity is limited to solar, and so the resulting model predictions.

A significant step further was made by the New Generation Spectral Library (NGSL) (Gregg et al. 2006), which was observed with the Imaging Spectrograph (STIS) onboard the Hubble Space Telescope (HST). The stellar spectra of the NGSL cover the range  $\sim 0.16\text{--}1.02 \mu\text{m}$  at resolution  $R \sim 1000$  and, therefore, unlike the IUE, it does not reach the Far-UV and it misses Ly $\alpha$ . However the 374 stars of this library have a good coverage of stellar atmospheric parameters, with metallicities between  $-2.0$  dex and  $0.5$  dex and spectral types from O to M for all luminosity classes. In Koleva & Vazdekis (2012) we determined the atmospheric parameters of this library in an homogeneous manner.

Here we make use of the NGSL to extend our stellar population models to the UV spectral range (Section 2). The computed SSP spectra are joined to those we predict for the visible (Vazdekis et al. 2010, as recently updated in Vazdekis et al. 2015) and redder spectral ranges (Vazdekis et al. 2012; Röck et al. 2015, 2016) to cover the

<sup>1</sup> <http://archive.stsci.edu/iue/>

range  $\lambda\lambda$  1680–50000 Å, at moderately high resolution, all based on empirical stellar libraries (Section 3). In Section 4 we focus on the behaviour of the colours, spectra and line-strength indices in the UV spectral range. In Section 5 we compare our models with other predictions in the literature. In Section 6 we compare our model predictions to stellar cluster and galaxy data. Finally, in Section 7 we summarize our main results and conclusions.

## 2 MODEL CONSTRUCTION

The models computed in this work employ scaled-solar isochrones and do not take into account the specific abundance element ratio of the stellar spectra. Therefore these models, for which we assume that  $[M/H] = [Fe/H]$ , can be considered "base" models. As the empirical stellar spectra follow the Milky-Way abundance pattern as a function of metallicity, the resulting base models are nearly consistent and scaled-solar around solar metallicity. However at low metallicity they lack consistency as these models combine scaled-solar isochrones with  $\alpha$ -enhanced stellar spectra. Note that in Vazdekis et al. (2015) we computed self-consistent models in the optical range, which are scaled-solar or  $\alpha$ -enhanced for all metallicities, with the aid of the theoretical stellar spectra of Coelho et al. (2005, 2007).

We employ the two sets of scaled-solar theoretical isochrones of Girardi et al. (2000) (hereafter Padova00) and Pietrinferni et al. (2004) (hereafter BaSTI). The Padova00 isochrones cover a wide range of ages, from 0.063 to 17.8 Gyr, and six metallicity bins ( $Z = 0.0004, 0.001, 0.004, 0.008, 0.019$  and 0.03), where 0.019 represents the solar value. The range of initial stellar masses extends from 0.15 to  $7M_{\odot}$ . In comparison to their isochrones published in Bertelli et al. (1994) the Padova00 employ an improved version of the equation of state, the opacities of Alexander & Ferguson (1994) and a milder convective overshoot scheme. A helium fraction was adopted according to the relation:  $Y \approx 0.23 + 2.25Z$ .

We also use here the BaSTI theoretical isochrones of Pietrinferni et al. (2004) supplemented by additional computations as described in Vazdekis et al. (2015), which include an extra (supersolar) metallicity bin, and extension of the isochrones to the very low-mass (VLM) regime down to  $0.1M_{\odot}$ , based on the models of Cassisi et al. (2000). We note that the temperatures for these stars are cooler than those of Padova00 (Vazdekis et al. 2012). For a complete description of the BaSTI database we refer the interested reader to Pietrinferni et al. (2004, 2006, 2009, 2013) and Cordier et al. (2007). We adopted the non-canonical BaSTI models with the mass loss efficiency of the Reimers law (Reimers 1977) set to  $\eta = 0.4$ . The initial He mass fraction ranges from 0.245 to 0.303, for the more metal-poor to the more metal-rich composition, respectively, with  $\Delta Y/\Delta Z \approx 1.4$ . The adopted BaSTI isochrones cover twelve metallicity bins:  $Z = 0.0001, 0.0003, 0.0006, 0.001, 0.002, 0.004, 0.008, 0.0100, 0.0198, 0.0240, 0.0300$  and 0.0400. For each metallicity, the isochrone age range covers the interval from 0.03 to 14 Gyr. We note that for the solar metallicity model set the atomic diffusion of both helium and metals was properly accounted for to be able to match accurately the helioseismological constraints. The best match to the depth of the convective envelope ( $0.716R_{\odot}$ ) of the present solar envelope He abundance

( $Y = 0.244$ ), and of the actual (Z/X) ratio [ $(Z/X = 0.0244)$ ], lead to an initial He abundance and metallicity ( $Y_{\odot} = 0.2734$ ,  $Z_{\odot} = 0.0198$ ).

There are differences among these two sets of isochrones. The MS loci are in good agreement. The TO stars have similar luminosity for old stellar populations, but their luminosities differ for young and intermediate age regimes. The BaSTI models provide systematically cooler (hotter) RGB at low (high) metallicity than the Padova00 models. The core He-burning stage is hotter for the BaSTI models for old populations, mostly due to differences in the adopted efficiency of mass-loss along the RGB. However, for young ages the Padova00 models show more extended blue loops, due to differences in the physical inputs and the treatment of convection of the He-burning core intermediate-mass stars. Finally, we note that both the Padova00 and BaSTI isochrones include the thermally pulsing AGB regime using simple synthetic prescriptions. However the contributions of these red stars are nearly negligible in the UV spectral range. We refer the interested reader to Cassisi et al. (2004), Pietrinferni et al. (2004) and Vazdekis et al. (2015) for a more detailed comparison of these two sets of isochrones.

None of these models include stellar rotation, which is particularly relevant for massive stars. Among other effects rotation brings more material to the convective core and therefore increases the MS lifetimes by as much as  $\sim 25\%$  and decreases the surface gravity and the opacity in the radiative envelope, raising the luminosity (Maeder & Meynet 2000). As a result of rotation the colours of the stellar populations with ages smaller than  $\sim 40$  Myr vary by 0.1 – 1 mag with respect to the non-rotating models, being this difference larger with increasing wavelength and increasing metallicity (Vázquez et al. 2007). Note that our BaSTI-based models reach 30 Myr and therefore the stellar rotation of massive stars, not included here, might have a non negligible effect on these young populations. Nevertheless we obtain reasonably good fits to the absorption line-strengths of LMC stellar clusters in this age regime, as discussed in Section 6.3.1.

The theoretical parameters of these isochrones are transformed to the observational plane to obtain stellar fluxes using empirical (rather than theoretical) relations between colours and stellar parameters ( $T_{\text{eff}}$ ,  $\log g$ ,  $[Fe/H]$ ). We use the metallicity-dependent relations of Alonso, Arribas & Martínez-Roger (1996) and Alonso, Arribas & Martínez-Roger (1999) for dwarfs and giants, respectively. Two extensive photometric stellar libraries of dwarfs and giants (around  $\sim 500$  stars each library) were employed to derive these temperature scales throughout the IR-Flux method, which is only marginally dependent on model atmospheres. We use the empirical compilation of Lejeune, Cuisinier & Buser (1997, 1998) (and references therein) for the coolest dwarfs ( $T_{\text{eff}} \lesssim 4000$  K) and giants ( $T_{\text{eff}} \lesssim 3500$  K) for solar metallicity, and also for stars with temperatures above  $\sim 8000$  K. We use a semi-empirical approach for the low temperature stars of other metallicities. For this purpose we combine these relations and the model atmosphere predictions of Bessell et al. (1989, 1991) and the library of Fluks et al. (1994). We also use the metal-dependent bolometric corrections of Alonso, Arribas & Martínez-Roger (1995) and Alonso et al. (1999) for dwarfs and giants, respectively, and adopt  $BC_{\odot} =$

-0.12. Assuming  $V_{\odot} = 26.75$  (Hayes 1985) we obtain for the sun the absolute magnitude  $M_{V_{\odot}} = 4.82$  and  $M_{\text{bol}_{\odot}}$  is given by  $M_{V_{\odot}} + \text{BC}_{V_{\odot}} = 4.70$ .

To compute the integrated spectrum of a single-age and single-metallicity stellar population, SSP, we integrate along the isochrone the stellar spectra of the NGSL library (Koleva & Vazdekis 2012), which is described in Section 2.1. Specifically, we follow the approach described in Vazdekis et al. (2015) for the base models. In this integration the number of stars in each mass bin comes from the adopted IMF, for which we assume four shapes as summarized in Vazdekis et al. (2003, 2015). These include the multi-part power-law IMFs of Kroupa (2001), i.e. universal and revised, and the two power-law IMFs described in Vazdekis et al. (1996), i.e. unimodal and bimodal, both characterised by the logarithmic slope,  $\Gamma$  and  $\Gamma_b$ , respectively, as a free parameter. In addition, in this work we also have implemented the Chabrier (2001) single-stars IMF. The Salpeter (1955) IMF is obtained by adopting the unimodal IMF with  $\Gamma = 1.35$ , and (although not identical) the Kroupa Universal IMF is very similar to a bimodal IMF with slope  $\Gamma_b = 1.3$ .

During the integration we scale the stellar spectra according to their fluxes in the  $V$  broad-band filter, which is fully contained in the NGSL stellar spectra. The predicted flux in this band is computed according to the same empirical photometric relations employed for the isochrones. To normalise the spectra we convolve with the filter response of Buser & Kurucz (1978). To obtain the absolute flux in the  $V$ -band we follow the method described in Falc3n-Barroso et al. (2011), which is based on the calibration of Fukugita, Shimasaku & Ichikawa (1995). We obtain the zero-point using the Vega spectrum of Hayes (1985) with a flux of  $3.44 \times 10^{-9} \text{ erg cm}^{-2} \text{ s}^{-1} \text{ \AA}^{-1}$  at  $5556 \text{ \AA}$ , and the  $V$  magnitude set to 0.03 mag, consistent with Alonso et al. (1995).

For each star, with a given set of atmospheric parameters, we use the spectra of the stars of the library with the closest parameters to apply the interpolation scheme described in Vazdekis et al. (2003) (see Appendix B), as updated in Vazdekis et al. (2015). This algorithm selects the stars whose parameters are within a box around the requested parametric point ( $T_{\text{eff}}$ ,  $\log g$ ,  $[\text{Fe}/\text{H}]$ ), which is divided in eight cubes, all with one corner at that point. If no stars are found in any of these cubes it can be expanded until suitable stars are found. This local interpolation algorithm is particularly suitable to overcome the limitations inherent to the gaps and asymmetries in the distribution of stars around that point. The larger the density of stars around it the smaller the box is, which can be as small as imposed by typical uncertainties in the determination of the parameters (see Cenarro et al. 2001b). We assign the smallest box to those parametric points for which the NGSL provided density values where the cumulative density fraction reached the upper 99.7 percentile. For example, this has been the case for stars with similar parameters to the sun, or solar metallicity giants with temperatures around 4800 K. In each of these cubes, the stars are combined taking into account their parameters and the signal-to-noise of their spectra. Finally, these combined stars are weighted to obtain the stellar spectrum with the requested atmospheric parameters.

It is worth noting that, within this integration scheme, a stellar spectrum is attached to the isochrones following

the requested stellar parameters ( $T_{\text{eff}}$ ,  $\log g$ ,  $[\text{Fe}/\text{H}]$ ), irrespective of the evolutionary stage. This is particularly relevant for the AGB phase in the intermediate-age regime, although these stars are more influential at redder wavelength ranges. More relevant to the UV is the evolution of binary (or multiple) stars, which we do not take into account in the models presented here. Furthermore we have decreased, and in some cases discarded, the spectroscopic binaries that are present in the library (see Section 2.1). However we provide models computed with the Kroupa Revised IMF (Kroupa 2001), which correct the relative number of stars for the systematic bias due to unresolved binary proportion. Very recently Hern3ndez-P3rez & Bruzual (2014) implemented in their stellar population models varying fractions of interacting binary pairs as progenitors of EHB stars to reproduce both UV-weak and UV-strong ETGs. In contrast, e.g., Smith, Lucey & Carter (2012), favour the metal-rich single-star origin to explain the UV flux excess in old stellar populations. The correlation found between the Far-UV colour and metallicity comes naturally within this scenario, as mass loss during the RGB phase increases with metallicity producing blue HB stars. To be able to properly contribute to this discussion we would need to extend the models to the Far-UV, which is mostly out of the reach of the spectral range covered by the NGSL stellar spectra implemented here. Note however that the IUE stellar spectral library is very useful for this purpose.

## 2.1 The stellar spectral library

The main ingredient employed for extending our models to the UV spectral range is the NGSL<sup>2</sup> (Gregg et al. 2006). The NGSL stars were observed with STIS on-board HST using three gratings (G230LB, G430L and G750L). The obtained spectra for each star overlap at  $2990 - 3060 \text{ \AA}$  and  $5500 - 5650 \text{ \AA}$ . The final spectra cover the wavelength range from  $\sim 0.16$  to  $\sim 1.02 \mu\text{m}$  (slightly different from star to star). The flux-calibration reaches a precision of 3 percent (Heap & Lindler 2009). The targeted stars (600) were chosen to sample four metallicity groups, with roughly 150 stars in each bin:  $[\text{Fe}/\text{H}] < -1.5$ ;  $-1.5 < [\text{Fe}/\text{H}] < -0.5$ ;  $-0.3 < [\text{Fe}/\text{H}] < +0.1$ ;  $+0.2 < [\text{Fe}/\text{H}]$ . However, about 200 stars were not observed due to the STIS failure in 2004.

In Koleva & Vazdekis (2012) we downloaded version 2 of the reduced data to determine in an homogeneous way the atmospheric parameters of the NGSL stars. For determining the stellar parameters we used the full spectrum fitting package *ULySS* (Koleva et al. 2009). We reached a precision for the FGK stars of 42 K, 0.24 and 0.09 dex for  $T_{\text{eff}}$ ,  $\log g$  and  $[\text{Fe}/\text{H}]$ , respectively. The obtained mean errors for the M stars were 29 K, 0.50 and 0.48 dex, and for the OBA stars 4.5 percent, 0.44 and 0.18 dex. In Koleva & Vazdekis (2012) we also determined the wavelength calibration precision and characterised the intrinsic resolution of the NGSL spectra. We find that the wavelength calibration is precise up to 0.1 px, after correcting a systematic effect in the optical range. The spectral resolution varies from  $3 \text{ \AA}$  in the UV to  $10 \text{ \AA}$  in the near-infrared (NIR), corresponding to a

<sup>2</sup> <http://archive.stsci.edu/prepds/stisngsl/>

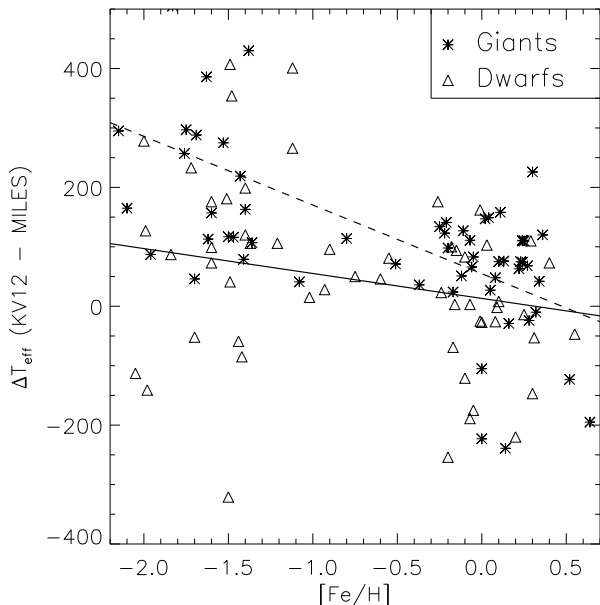


**Figure 1.** Temperature difference obtained by comparing the values of Koleva & Vazdekis (2012), quoted as KV12, with those of MILES (Cenarro et al. 2007a) as a function of metallicity for the stars in common between these two libraries. The obtained fits for dwarf (open triangles) and giant (asterisks) stars are shown in solid and dashed lines, respectively (see Eq. 1).

roughly constant reciprocal resolution  $R = \lambda/\delta\lambda \approx 1000$  and an instrumental velocity dispersion  $\sigma_{ins} \approx 130 \text{ km s}^{-1}$ .

In Koleva & Vazdekis (2012) we estimated the Galactic extinction for each of the stellar spectra. In brief, this was performed when deriving the fundamental parameters of the NGSL stars as we fit their spectra with interpolated templates (e.g. MILES stars) together with a multiplicative polynomial. As both the flux calibration of the employed spectra and the derived atmospheric parameters are accurate, we use this polynomial to estimate the Galactic extinction, which is obtained by fitting the multiplicative polynomial to the Fitzpatrick (1999) law. To correct from Galactic extinction the individual stellar spectra we divided them by this fit, and extended it to the blue and red wavelengths. We refer the interested reader to Koleva & Vazdekis (2012) for an extensive description of the method.

To be implemented in our models we rebinned the original spectra, with varying sampling, namely  $1.373 \text{ \AA/px}$  ( $\lambda\lambda 1675 - 3060 \text{ \AA}$ ),  $2.744 \text{ \AA/px}$  ( $\lambda\lambda 3060 - 5650 \text{ \AA}$ ) and  $4.878 \text{ \AA/px}$  ( $\lambda\lambda 5650 - 10196 \text{ \AA}$ ) to a constant value of  $0.9 \text{ \AA/px}$ , i.e., similar to MILES, for the whole spectral range. The spectra are calibrated in air wavelengths. Note however that only the first two spectral ranges are considered here for the models described in Section 3.

All the stars were visually inspected, one by one, by comparing them to stars with similar parameters and to the output of the interpolator, once excluding the target spectrum, following the method described in Vazdekis et al. (2010). The two approaches allowed us to identify stars whose spectra clearly deviate from the expected shape, either globally or within some specific wavelength range. We

employed for the models 303 stars from the original sample composed of 374 stars. Nearly half of the removed stars are spectroscopic binaries that were found to be redundant, as there are other stars with very similar parameters in the library. Other reasons for removing stars include strong emission along the whole spectral range, unexpected dips in flux, wrong spectrum shape for the estimated parameters and some very peculiar stars. Finally, instead of removing 15 stars, whose spectra were partially affected by some of these problems, we decreased their weight for stellar population modeling by means of the interpolation scheme we applied to synthesize the requested stars. Among them are hot stars showing interstellar absorption lines affecting, e.g., the MgII feature at  $\sim 2800 \text{ \AA}$ , as the modest resolution of the NGSL spectra does not allow us to properly deal with them. This has also been the case for very cool stars showing chromospheric emission filling in this feature (e.g. Génova et al. 1990). This choice of decreasing the weight of these stars is mainly motivated by the fact that their parameters were difficult to match by the remaining, cleaner, stars, and we wanted to avoid increasing the number of local gaps in our stellar parametric distribution.

We also performed cosmetic corrections to the spectra of 53, mostly red, stars. In many cases where we found some negative flux values, typically blueward  $\sim 2150 \text{ \AA}$  where the S/N gets very low (in all cases  $< 20$  for the spectrum obtained with the blue grating of STIS, i.e.  $\lambda < 3060 \text{ \AA}$ ), we assigned the minimum positive flux value within a  $20 \text{ \AA}$  wide window that is centered on that pixel(s). For 20 of these stars, i.e. mostly the coolest ones, we found that significant portions of their spectra blueward  $\sim 2150 \text{ \AA}$  showed too noisy spectrum, including many negative flux values. Therefore we just assigned the mean flux measured in the neighbouring, redder,  $100 \text{ \AA}$  wide window, which is located between  $2150$  and  $2400 \text{ \AA}$ , depending on each star. Note that the contributions of these stars in the UV spectral region is negligible.

To match our NGSL-based models to those computed in the optical range (see Section 3), we need to homogenize the Koleva & Vazdekis (2012) stellar parameters with our reference values adopted in the MILES library (Cenarro et al. 2007a). For this purpose we compared the parameters of the NGSL stars in common with MILES. Fig. 1 shows the difference in temperature obtained as a function of metallicity for the dwarf and giants stars. Although there is a significant scatter throughout the whole metallicity range, we see that the temperature difference increases with decreasing metallicity and that this effect is larger for the giants (we refer the interested reader to Koleva & Vazdekis 2012 for further details on these differences). The obtained fits allowed us to transform these temperatures to the MILES system by applying the following corrections:

$$\begin{aligned} T_{\text{MILES}} &= T_{\text{KV12}} - 13.1784 - 41.9432[\text{Fe}/\text{H}] & (\text{dwarfs}) \\ T_{\text{MILES}} &= T_{\text{KV12}} - 54.7807 - 115.537[\text{Fe}/\text{H}] & (\text{giants}) \end{aligned} \quad (1)$$

For 109 stars in common with MILES and 15 stars in common with the CAT library (Cenarro et al. 2001b), which is also in the same system as MILES, we adopted the parameters provided by these libraries. For 168 stars we corrected the parameters of Koleva & Vazdekis (2012) according to Eq. 1. Finally, for 10 stars in common with MILES (HD 10380, HD 37828, HD 44007, HD 95735,

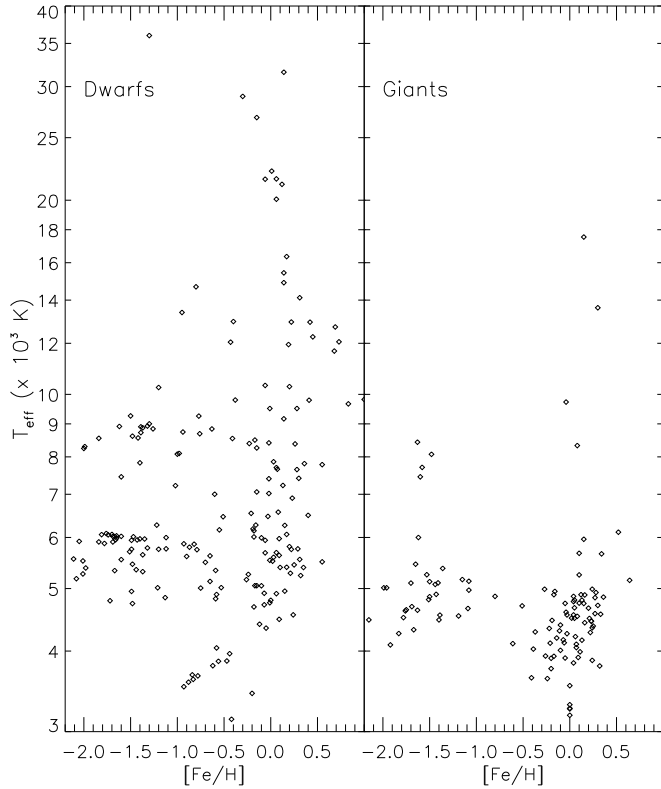


**Figure 2.** Adopted atmospheric parameters for the NGSL stars. Dwarf stars are shown in the left panel whereas the giants are shown in the right panel.

HD 112413, HD 123657, HD 164353, HD 167006, HD 175865, BD +37 1458 and BD +44 2051) and one in common with CAT (BD +44 205) we did not use the parameters listed in these libraries as we found that those of [Koleva & Vazdekis \(2012\)](#), transformed in this way, matched better other stars with similar parameters.

The resulting stellar parameters are shown in Fig. 2. Dwarf stars with temperature in the range 4500–9000 K are well covered within the metallicity range  $-1.7 < [\text{Fe}/\text{H}] < +0.3$ . The poor coverage of cool dwarfs is not a problem, since their contribution to the total light in the UV is small. Similarly the number of hot dwarfs decreases significantly with increasing temperature, limiting the reliability of our model predictions for ages smaller than  $\sim 0.5$  Gyr. We also see that the highest density of stars is obtained for solar metallicity. This also applies to the giants as illustrated by the right panel of the figure. Note that for some of the coolest giant stars with metallicity estimates around  $-1$  dex we do not take their metallicity into account. Instead we set their metallicity to 0.0 to optimize the interpolation in this sparsely populated very low temperature regime. However there is a large gap in the coverage of giants with  $[\text{Fe}/\text{H}] < -0.3$ , with some improvement around  $[\text{Fe}/\text{H}] < -1.7$ . This gap prevents us of building stellar population models in spectral regions dominated by these redder stars. The model limitations imposed by these gaps are discussed in detail in the next section.

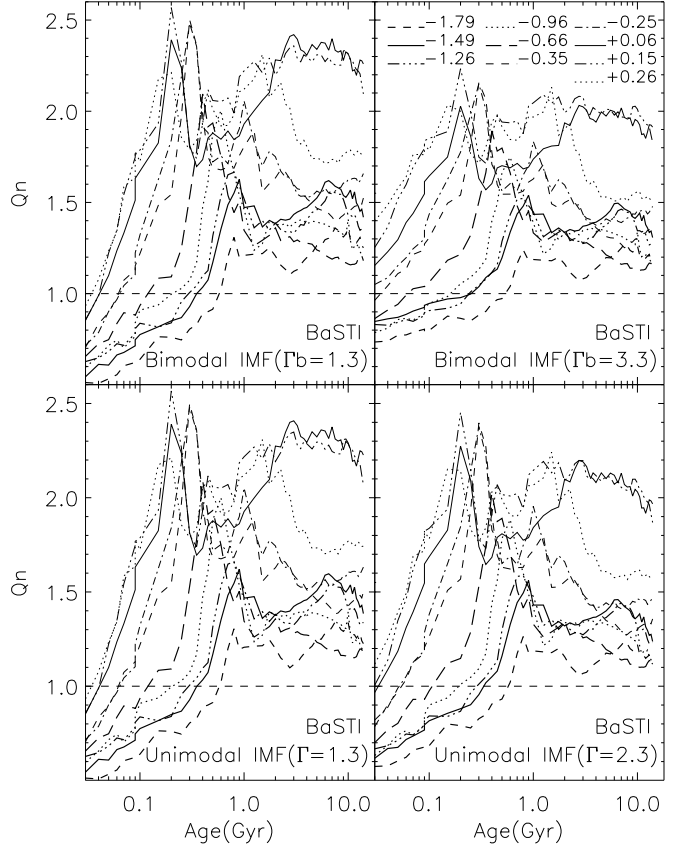


**Figure 3.** The normalized quality parameter,  $Q_n$ , of the NGSL based SSP spectra computed with BASTI isochrones is plotted as a function of age for various metallicities as indicated within the upper-right panel. Models can be considered safe for  $Q_n > 1$ . The upper-left panel shows the quality of the models computed with a bimodal IMF with slope 1.3, whereas a rather bottom-heavy IMF with slope 3.3 is shown in the upper-right panel. The  $Q_n$  values corresponding to the models computed with a Unimodal IMF with slope 1.3 (i.e. Salpeter) and 2.3 are shown in the bottom-left and bottom-right panels, respectively.

## 2.2 Quality of the UV SSP spectra

To estimate the quality of the SSP spectra in the UV range we follow the quantitative approach introduced in [Vazdekis et al. \(2010\)](#), which makes use of the interpolation algorithm described in Section 2. We compute a normalised quality parameter,  $Q_n$ , which is related to the density of stars around the atmospheric parameters of the stars that are requested when integrating along the isochrone. Basically, the higher these densities are in the NGSL, the higher the  $Q_n$  value of the resulting SSP spectrum. To obtain  $Q_n$  we normalise it with respect to a minimum acceptable value, which comes from a poor, but still acceptable, parameter coverage. We refer the interested reader to [Vazdekis et al. \(2010\)](#) for a full description of the method. The main difference, apart of the use of the NGSL, is that we use the flux in the U band for the weighting of the stars required to compute this parameter (see Equation 5 of [Vazdekis et al. 2010](#)). This is motivated by the fact that we only will use the UV spectral region of these models (see Section 3).

Fig. 3 and Fig. 4 show the resulting  $Q_n$  values for the

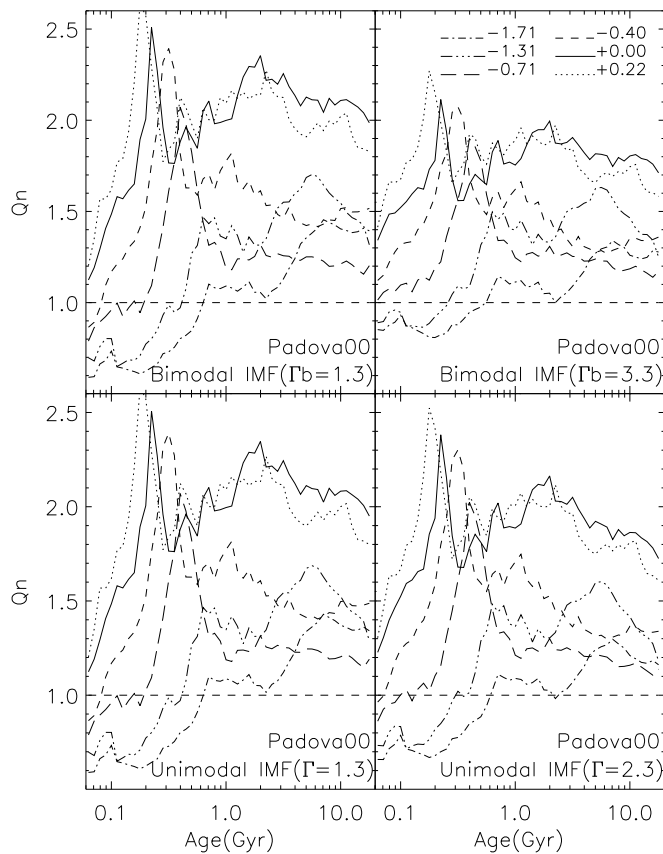


**Figure 4.** Same as Fig. 3, but for the models computed with the Padova00 isochrones.

models computed on the basis of the BaSTI and Padova00 isochrones. Models for which  $Q_n > 1$  can be considered acceptable, whereas the ones with values slightly lower than one can still be used with some caveats, depending on the applications such as, e.g. colours. These two figures show that the models are safe for all the plotted metallicities for ages above  $\sim 0.5$  Gyr. For metallicities around solar these models are safe for younger ages, particularly when steepening the IMF, as illustrated in the right panels. For intermediate-aged stellar populations we observe a relative increase of the  $Q_n$  values as a result of the fact that in our interpolation scheme we do not consider the metallicity of the stars for temperatures above  $\sim 9000$  K. The largest  $Q_n$  values are obtained for the models with metallicities around solar. The quality of the models with  $[M/H] \sim 0.2$  drops significantly due to the poorer coverage of stars with supersolar metallicities in the NGSL. The quality of the models also decreases for low metallicities. It is not surprising that for the old stellar populations the lowest  $Q_n$  values are obtained for metallicities around  $[M/H] \sim -0.7$ . This result is consistent with the scarce coverage of stars with metallicities around such value, as shown in Fig. 2.

Fig. 3 and Fig. 4 also show a peculiar behaviour of the  $Q_n$  parameter as a function of IMF slope. For intermediate- and old-aged stellar populations the quality decreases slightly when steepening the IMF. In contrast, for the models with the youngest ages a bottom-heavier IMF contributes to increase the value of the quality parameter. Such a behaviour

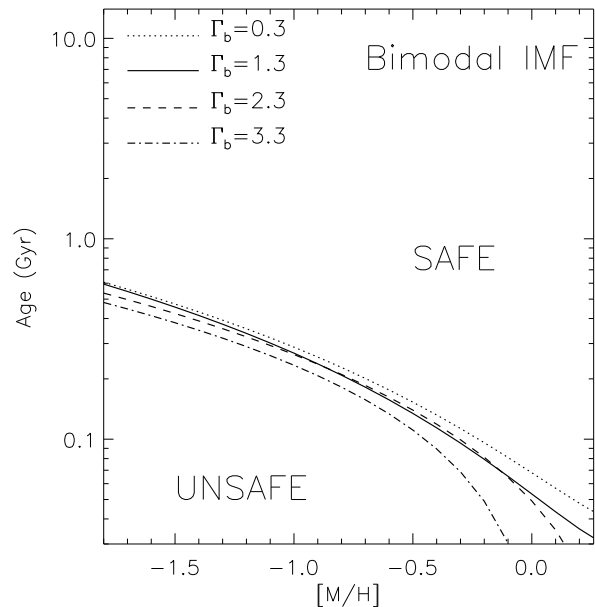


**Figure 5.** Safe and unsafe models with bimodal IMF and varying slopes as marked within the plot. The safe age and metallicity ranges showed here refer to the UV spectral range and apply to the models computed with the two sets of isochrones feeding our models. See the text for details.

can be understood by tracking the density of stars along the temperature axis in the left panel of Fig. 2. For old stellar populations and bottom-heavy IMFs the contribution to the total light of MS dwarfs with  $T_{\text{eff}} \lesssim 4500$  K increases relatively to the hotter stars, compared to a standard IMF. As the density of such cool stars is lower in the NGSL library, the resulting  $Q_n$  values decrease. On the contrary, for the stellar populations with the youngest ages the relative contribution of stars with  $T_{\text{eff}} \gtrsim 10000$  K (less abundant) with respect to the MS stars of lower temperature (more abundant) decreases when the IMF becomes bottom-heavier.

Finally, in Fig. 5 and Fig. 6 we summarize the safe and unsafe SSPs in the UV spectral range for the models with bimodal and unimodal IMF types, respectively. The plotted curves, which correspond to different IMF slopes, were obtained by fitting the age/metallicity corresponding to models with  $Q_n$  values around 1 and therefore these ranges must be taken with some caveats. Note that the Salpeter IMF safe/unsafe ranges are well represented by the curve corresponding to the unimodal case with slope 1.3, whereas the ones for the Kroupa and Chabrier IMFs are very close to the bimodal case with slope 1.3.

### 3 E-MILES: THE EXTENDED MILES MODELS

In Section 2 we have described how we compute the models in the NUV making use of the NGSL stellar library, which extend to the red out to  $\sim 1 \mu\text{m}$ . However we only use from these models the spectral region blueward  $3540 \text{ \AA}$ , which is joined to the blue end of the SSP spectra based on the MILES stellar library. These models have been recently

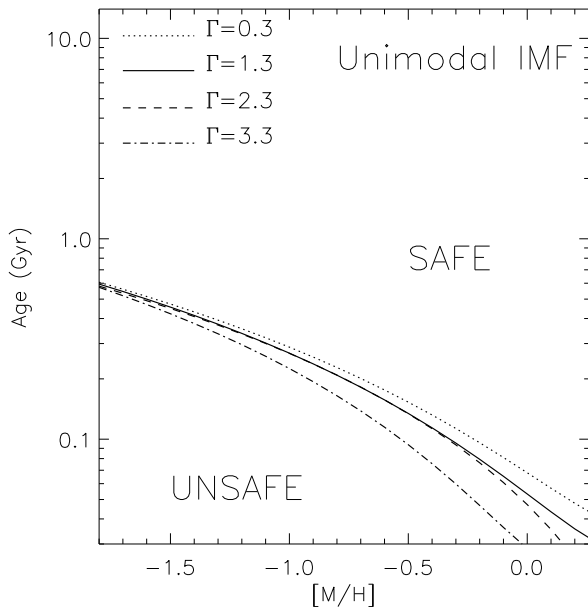


**Figure 6.** Same as Fig. 5, but for models adopting a unimodal IMF with various slopes as quoted within the plot.

extended to the near-IR (Röck et al. 2016) by joining the MIUSCAT SSP spectra (Vazdekis et al. 2012), which apart of MILES also employ the Indo-US (Valdes et al. 2004) and CaT (Cenarro et al. 2001a) stellar libraries, to the SSP spectra computed on the basis of the IRTF stellar library (Cushing et al. 2005; Raynier et al. 2009) reaching out to  $5\mu\text{m}$  (Röck et al. 2015). All these models were computed with our population synthesis code in a fully consistent manner. The chief aspect of these models is that the resulting SSP spectra are based on empirical stellar spectral libraries throughout the whole spectral range,  $\lambda\lambda 1680.2\text{Å} - 49999.4\text{Å}$ , at moderately high resolution.

To join our newly synthesized NUV SSP spectra to those computed in the MILES range we have followed a similar procedure to the one adopted for building the MIUSCAT SSP spectra (Vazdekis et al. 2012). For this purpose we identified a spectral region  $\lambda\lambda 3541.4 - 3566.6\text{Å}$ , where no major features are found for the range of ages and metallicities covered by our models<sup>3</sup>. This overlapping window has been chosen to be sufficiently wide to reach enough statistics for the continuum counts and, at the same time, to avoid the presence of strong spectral features. To join the two models, we have re-scaled the NGSL based SSP spectra to match the continuum of the models based on MILES within this pseudo-continuum window. To compare the two fluxes in this window, we smoothed the MILES SSP spectra to  $5\text{Å}$  to match the nominal resolution of our NGSL based models in this specific spectral range (see Koleva & Vazdekis 2012). Note that in the combined models we do not change the nominal resolutions of the NGSL and MILES based SSP

<sup>3</sup> For the E-MILES models we avoided to use the small spectral range extension blueward MILES, down to  $3464.9\text{Å}$ , of the MIUSCAT models based on the Indo-US stellar library.

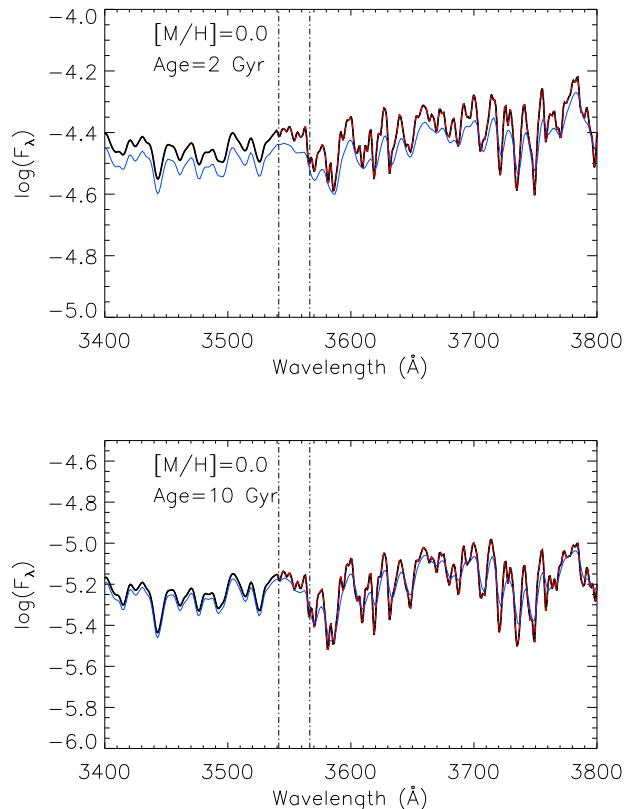


**Figure 7.** The vertical lines mark the selected pseudo-continuum for joining the NGSL- and MILES-based models. The thick black line represents the combined SSP spectrum and the thin blue (thick red) ones represent the NGSL (MILES) SSP. The panels show two representative SSP ages, 2 (upper panel) and 10 Gyr (lower panel) and solar metallicity.

spectra. A zoom of the combined models in the matching region is shown in Fig. 7 for two representative SSPs. Note that the flux calibration of NGSL and MILES models are in good agreement (within 0.02 mag), particularly for the old SSP model (lower panel). Therefore the joining is possible by only slightly adjusting fluxes in the selected overlapping window. This has been possible due to the good flux calibration of the stellar spectra of both MILES and the NGSL in this spectral range. Thus, we ended up covering the wavelength range from  $1680.2$  to  $49999.4\text{Å}$ . Note the drop in resolution from  $5$  to  $2.51\text{Å}$ , blueward  $3541.4\text{Å}$ , is clearly visible in Fig. 7.

The E-MILES models are computed for both BaSTI and Padova00 isochrones and five IMF shapes: Kroupa Universal, Revised Kroupa, Chabrier, Unimodal and Bimodal. For the latter two functional forms the slope has been varied from very top-heavy IMF slope (0.3) to very bottom-heavy (3.3). Table 1 lists the resolutions of the various spectral ranges covered by the combined models. Note that blueward  $8950\text{Å}$  the models have a constant FWHM, whereas for redder wavelengths  $\sigma$  is constant. Fig. 8 illustrates the resolution of the E-MILES spectra as a function of wavelength, both in FWHM and  $\sigma$ . All these models can be retrieved from the MILES website <http://miles.iac.es>, which also



**Table 1.** Spectral properties of the E-MILES models.

Units	$L_{\lambda}/L_{\odot}\text{\AA}^{-1}M_{\odot}^{-1}$ , $L_{\odot} = 3.826 \times 10^{33}\text{erg.s}^{-1}$
Continuum shape	Flux-scaled
Spectral range	$\lambda\lambda$ 1680.2 – 49999.4 $\text{\AA}$ (air-wavelengths)
Linear dispersion	0.9 $\text{\AA}/\text{pix}$
Spectral resolution	FWHM= 3.0 $\text{\AA}$ (1680.2 – 3060.8 $\text{\AA}$ ) <sup>a</sup> FWHM= 5.0 $\text{\AA}$ (3060.8 – 3541.4 $\text{\AA}$ ) <sup>a</sup> FWHM= 2.51 $\text{\AA}$ (3541.4 – 8950.4 $\text{\AA}$ ) <sup>b,c,d,e</sup> $\sigma = 60\text{ km s}^{-1}$ (8950.4 – 49999.4 $\text{\AA}$ ) <sup>f,g</sup>

<sup>a</sup>This work

<sup>b,c,d,e</sup>Vazdekis et al. (2003, 2010, 2012, 2015)

<sup>f,g</sup>Röck et al. (2015, 2016)

**Table 2.** Spectral windows employed for joining the various ranges of the E-MILES models

Window ( $\text{\AA}$ )	Spectral resolution variation	Modified spectrum shape	Reference
3541.4 – 3566.6	From FWHM= 5 $\text{\AA}$ to FWHM= 2.5 $\text{\AA}$	No, only flux shift applied	This work
7360.0 – 7385.0	FWHM= 2.5 $\text{\AA}$ constant	Yes	Vazdekis et al. (2012)
8390.0 – 8415.0	FWHM= 2.5 $\text{\AA}$ constant	Yes	Vazdekis et al. (2012)
8950.0 – 9100.0	From FWHM= 2.5 $\text{\AA}$ to $\sigma = 60\text{ km s}^{-1}$	Yes	Röck et al. (2016)

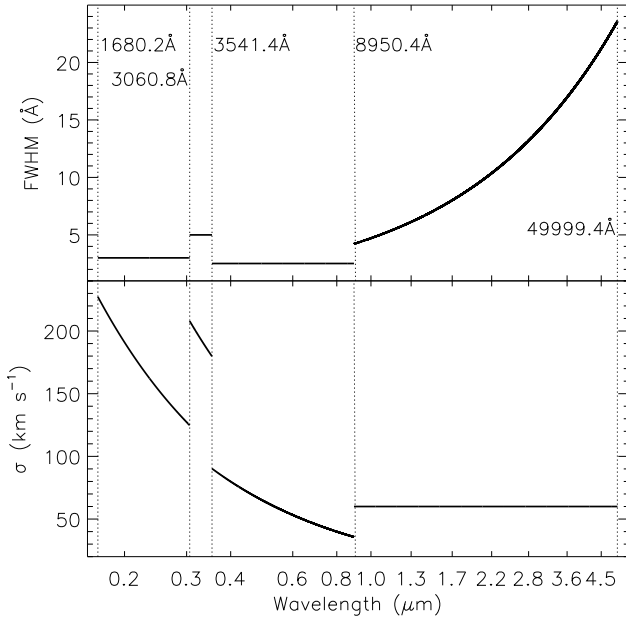


**Figure 8.** E-MILES spectral resolution as a function of wavelength both in FWHM (upper panel) and  $\sigma$  (lower panel). The vertical dotted lines indicate the exact wavelength values where the resolution changes. Versions of these models both at their nominal resolutions and smoothed to match a constant resolution (FWHM and  $\sigma$ ) are available on the MILES website.

includes versions of these models smoothed to match a constant resolution (FWHM and  $\sigma$ ) along the covered spectral range.

The quality parameter of the models in the spectral region blueward the MILES range has been discussed in Section 2.2. To assess the reliability of the models in the various spectral ranges we refer the reader to the specific papers

listed in Table 1. The E-MILES SSP spectra can be considered safe along the whole spectral range as restricted by the quality of the models redward 8950  $\text{\AA}$ . These models employ 180 carefully selected and prepared empirical stellar spectra from the IRTF library, which encompass cool supergiants and dwarfs as well as AGB and some carbon stars. However since the stars of the IRTF library are mostly bright, nearby stars of around solar metallicity, these models are most accurate in the metallicity range  $-0.40 < [\text{Fe}/\text{H}] < +0.20$  for ages above 1.5 Gyr.

There is a very important caveat to take into account for those users of E-MILES SEDs who aim at measuring or defining line-strength indices. It should be avoided line indices whose feature/pseudocontinuum bandpasses are located at either side of the joining spectral regions corresponding to the various SSP spectra employed for the combined E-MILES models. The index strength could vary as a result of the flux correction applied to match the two spectral regions. In addition it has to be taken into account that for some of these cases the resolution changes. These joining regions are located around  $\sim 3540, 7410, 8350$  and  $8950\text{\AA}$ . Table 2 lists these spectral windows with the corresponding resolutions, as well as an indication on whether the spectrum shape has been modified.

The resulting E-MILES spectra for two representative SSPs with age 12 Gyr and with metallicity  $[\text{M}/\text{H}] = +0.06$  and  $[\text{M}/\text{H}] = -0.35$  are shown in Fig. 9. Similarly, in Fig. 10 we show two representative models with age 2 Gyr. Finally, in Fig. 11 we illustrate the effect of the IMF for an old model of nearly solar metallicity. The selected IMF slopes can be considered representative for low- and high-mass ETGs, following the results of La Barbera et al. (2013). All the SSP spectra plotted in these three figures can be considered safe within the whole spectral range covered by the E-MILES models, i.e.  $\lambda\lambda$  1680.2–49999.4  $\text{\AA}$ .

The SSP models plotted in these three figures, including the youngest ones, show many absorption features in the UV spectral range. In general these features become stronger with increasing age and metallicity, as is the case for most

optical metallicity indicators. However metal line blanketing is significantly larger in the UV than in the optical range. This makes it very difficult to define reasonably well behaved index pseudocontinua bandpasses that are needed to measure the strengths of the main absorption lines. In fact the deepening and overlapping of metal lines surrounding some strong features might cause their strengths to decrease with increasing age/metallicity. This is the case of, e.g., the MgII feature at 2800 Å (Smith et al. 1991). Moreover this feature is part of a strong Mg lines complex that also includes the MgI feature centered on 2852 Å, which originates a prominent break at  $\sim 2920$  Å and a rather wide spectral dip. This dip, which is characteristic of cool stars and evolved stellar populations, is quantified by the so called Mg wide index (Fanelli et al. 1990), and can be used to study, e.g., higher redshift galaxies for which is not possible to obtain high S/N spectra. Similarly, the break seen at  $\sim 2600$  Å is caused by a complex dominated by Fe lines. As the spectral breaks bracketing these dips become more prominent with increasing age and metallicity they can be used as indicators to constrain these parameters. In fact Fanelli et al. (1990) proposed specific indices composed by a single pseudo-continuum and a feature bandpass to quantify these jumps, namely 2609/2660 and 2828/2921. Note also that there are specific features that are only noticeable in certain age/metallicity regimes. These include pseudo-continua that may look as emission like features, such as, e.g. that at  $\sim 2000$  Å, which is mostly seen in the more metal-rich model plotted in Fig. 10, as the surrounding absorption lines deepen with increasing metallicity. Note also the trough seen blueward 2100 Å that is characteristic of evolved metal-rich stellar populations (see Fig. 9), such as massive elliptical galaxies. In Section 4.3 we describe in detail the behaviour of the most prominent line indices in the UV spectral range covered by our models.

#### 4 BEHAVIOUR OF THE MODELS IN THE UV SPECTRAL RANGE

In this section we focus on the behaviour of the colours, spectra and line-strengths of our SSP models in the UV spectral range. We refer the reader to the specific papers listed in Table 1 for a detailed description of the behaviour of our models in other wavelength ranges.

##### 4.1 Colours

The flux calibration of the resulting SSP model spectra can be tested by comparing the synthetic U-B colour with our photometric predictions, which were computed on the basis of the extensive photometric stellar libraries described in Section 2. The U filter covers the overlapping region between the NGSL and MILES at  $\sim 3540$  Å, whereas the B filter is entirely measured within the MILES spectral range. The synthetic U-B colour is calculated using the Buser & Kurucz (1978) filter definitions and the Vega magnitude system (see Falcón-Barroso et al. 2011 for further details). The photometrically predicted colour is from Vazdekis et al. (1996) as updated in Vazdekis et al. (2010), and is based on empirical relations between colours and stellar parameters (Alonso et al. 1996, 1999). The residual U-B

colour shown in Fig. 12 is within typical zero-point errors ( $\sim 0.02$  mag) for the old models with solar metallicity. In this case the largest residuals are found for the intermediate age regime. However for the most metal-poor models ( $[M/H] = -1.71$ ) we obtain significantly larger residuals. It is worth recalling that, as discussed in Vazdekis et al. (2012) and Ricciardelli et al. (2012), the synthetic U magnitude is very sensitive to the definition of the U filter and the empirical colour-temperature relations used for the U-B colour are not as homogenous as in the other pass-bands, which makes it more difficult to match. We conclude that the inclusion of the NGSL model spectra has allowed us to obtain a significantly better agreement between the synthetic and photometric colours than what was achieved with the MIUSCAT model spectra alone (see Fig. 8 of Vazdekis et al. 2012).

The spectral range covered by our models allows us to measure the GALEX NUV magnitude. Figure 13 shows the theoretical predictions for the NUV-V colour synthesized from our models, both based on the Padova00 and BaSTI isochrones, as a function of age and metallicity. The NUV-V colour is given in the AB system, using the NUV GALEX transmission curve and the V broad-band filter of Buser & Kurucz (1978). Similarly to the optical colours the NUV-V reddens with increasing metallicity. However in comparison to the U-B colour (see Fig. 12) and the other optical colours, which tend to increase more modestly for ages above 1 Gyr, the NUV-V colour shows a steady and sharp increase with increasing age. Such a behaviour can be attributed to the strong contribution of the turnoff stars and the low contribution of the RGB phase in the NUV spectral range. For sub-solar and very metal-poor populations, the BaSTI-based models show a drop in colour for ages larger than 10 Gyr. This effect is more modest in the Padova00-based models as the Horizontal-Branch is cooler for such old ages.

The dependence of the NUV-V colour on the IMF slope is shown in Figure 14 for the bimodal IMF type. The figure shows the colour residual obtained for models with varying slope when compared to the reference standard model with  $\Gamma_b = 1.3$ . Solar metallicity models and two representative SSP ages are shown. The impact of the IMF on the UV colour appears negligible, i.e. well below typical zero-point errors, for the two ages. We conclude that the IMF has little effects in this spectral range.

##### 4.2 Spectra

We plot in Fig. 15 the UV range of a set of representative SSP spectra with young age (0.1 Gyr) and varying metallicity. Note that the strong flux variation within this wavelength range requires plotting the model spectra in various windows to be able to appreciate the features. The flux increases toward the shortest wavelengths. This effect is more pronounced for the more metal-poor stellar populations. Such an effect is attributed to the contribution of the turnoff stars, which become hotter with decreasing metallicity.

In Fig. 16 we show SSP spectra of models with intermediate age (1 Gyr) and varying metallicity. In this case two windows are sufficient to visualize the details of the spectra as the spectrum shape is flatter than in the models shown in Fig. 15. Note that for this age the models with the lowest metallicities still show an increasing flux for the bluest

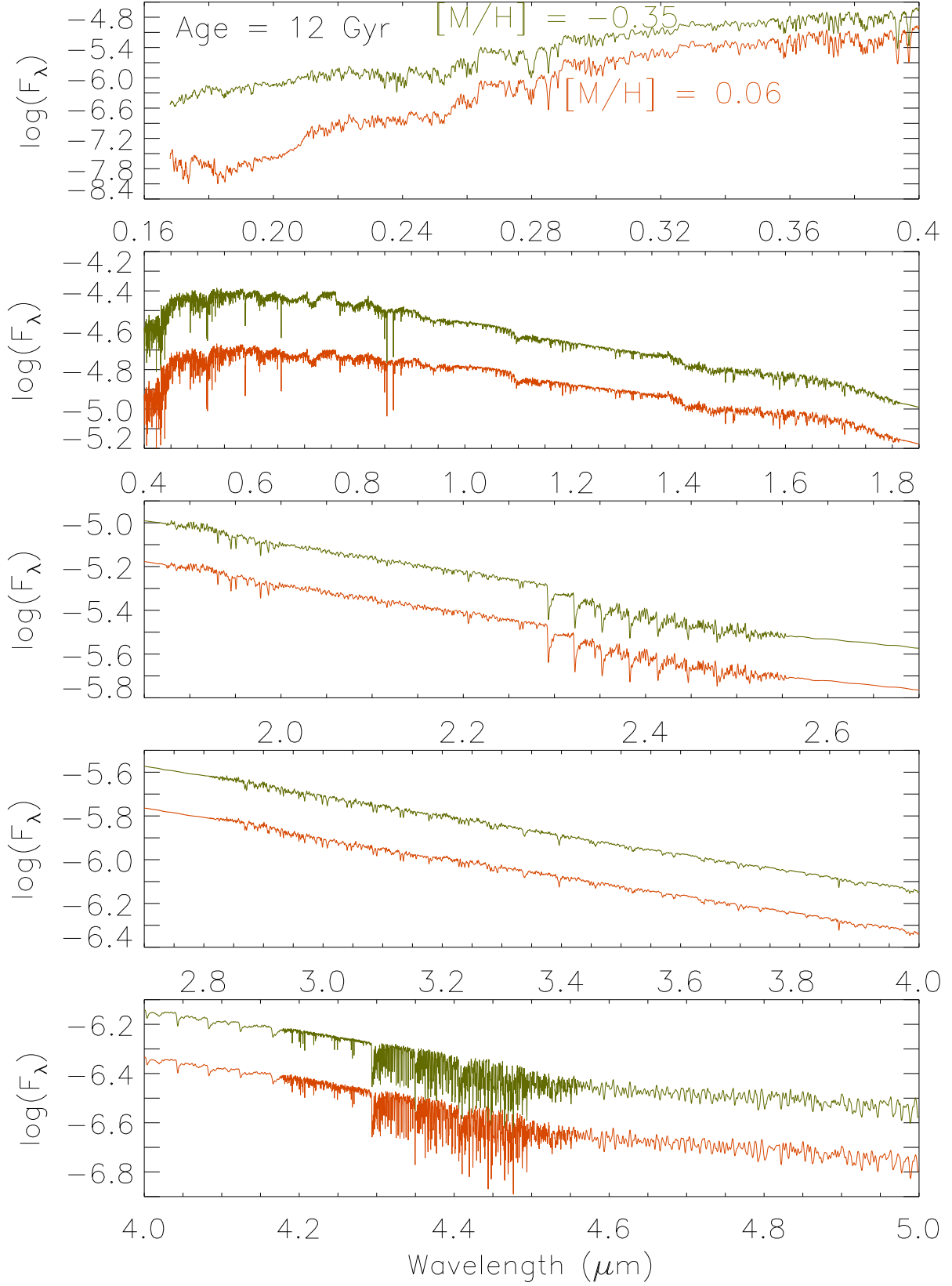


**Figure 9.** E-MILES SSP spectra with age 12 Gyr and Kroupa Universal IMF, computed with BaSTI, for two metallicity values:  $[M/H] = +0.06$  (orange) and  $[M/H] = -0.35$  (olive green). The model with subsolar metallicity has been shifted by  $\Delta \log F_\lambda = 1.5$  for visibility.

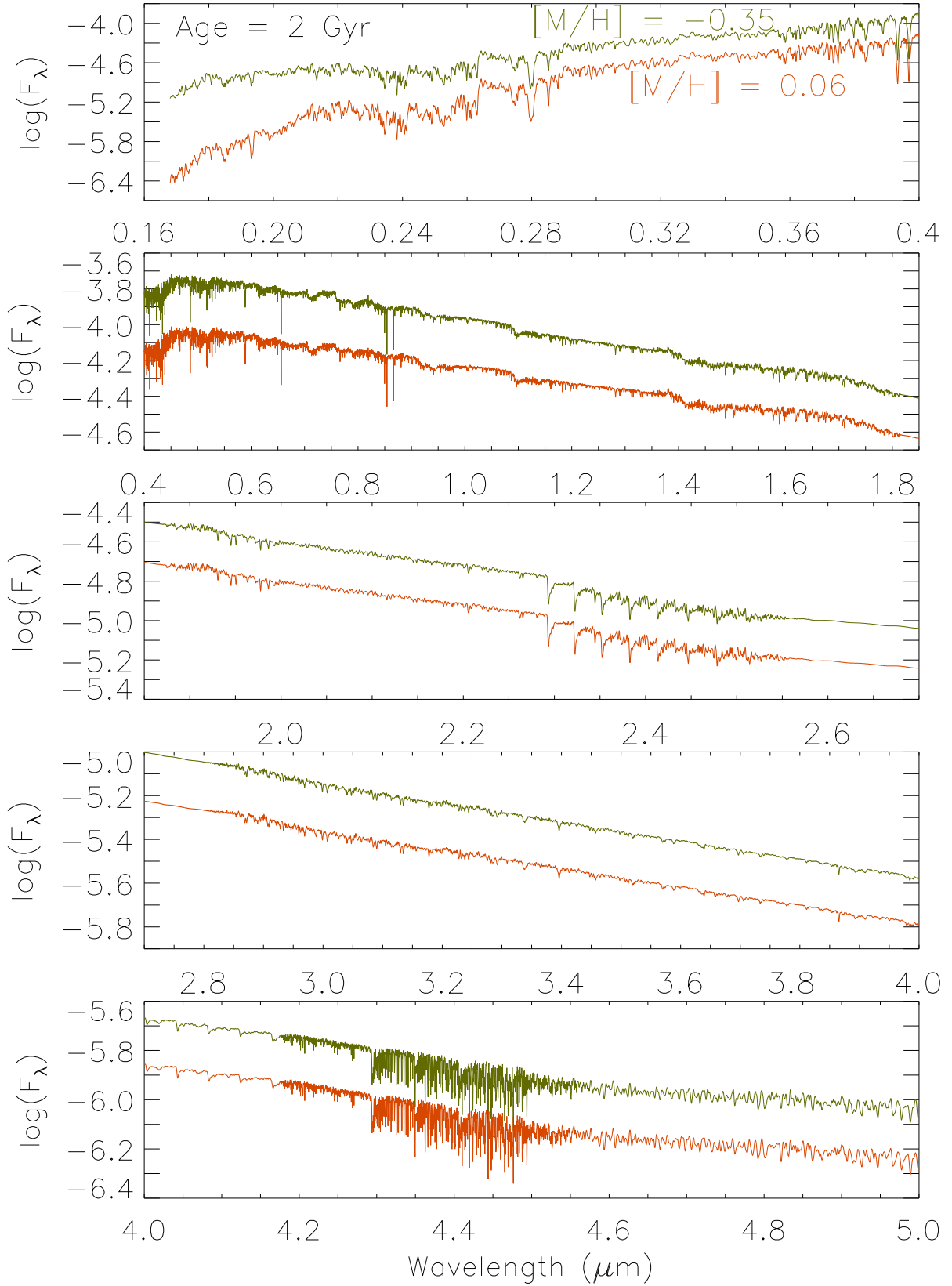


**Figure 10.** Same as in Fig. 9 but for models with age 2 Gyr. The model with subsolar metallicity has been shifted by  $+\Delta \log F_\lambda = 1.5$  for visibility.

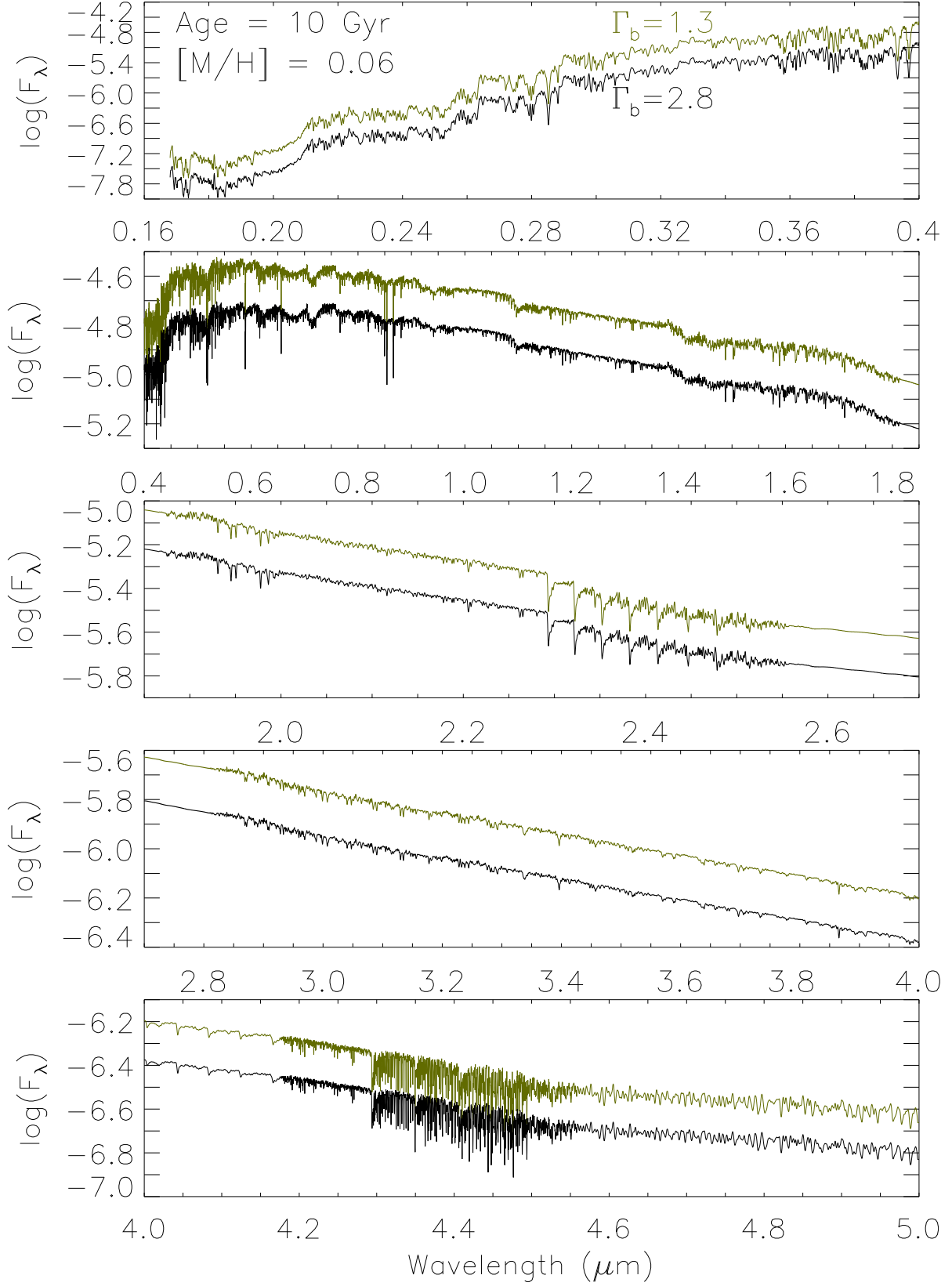


**Figure 11.** E-MILES SSP spectra of with age 12 Gyr, metallicity  $[M/H] = +0.06$  and bimodal IMF with slope  $\Gamma_b = 1.3$  (olive green) and  $\Gamma_b = 2.8$  (black). The model with  $\Gamma_b = 1.3$  has been shifted by  $+\Delta \log F_\lambda = 2.0$  in the first (upper) panel and by  $+\Delta \log F_\lambda = 1.3$  in all the other four panels for better visibility.

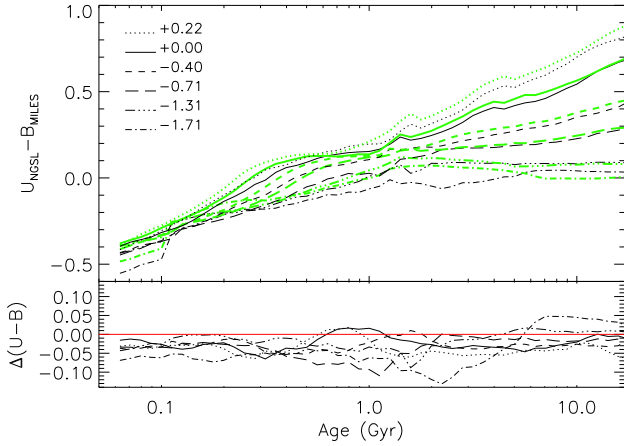


**Figure 12.** Time evolution of the U-B colour synthesised from our SSP model spectra (black lines), based on the Padova00 isochrones, and from our photometric predictions (light green thick lines) based on extensive photometric stellar libraries (see the text for details). The metallicity values of the SSPs are represented with varying line types as quoted within the upper panel. The lower panel shows the residual colour, i.e. synthetic minus photometric colour.

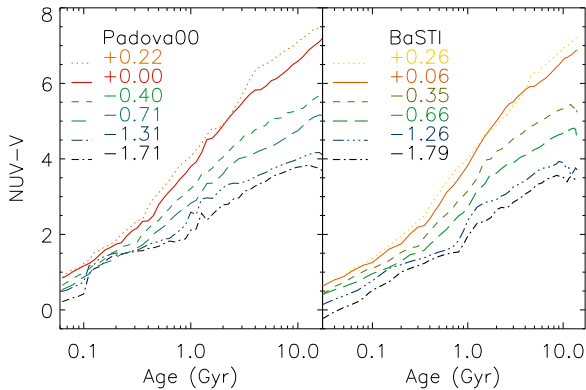


**Figure 13.** Evolution with time of the NUV-V colour synthesised from our SSP model based on Padova00 (left-hand panel) and BaSTI (right-hand panel) isochrones. The metallicities are represented with varying colour and line types as quoted within the panels.

wavelengths, whereas the most metal-rich SSPs become significantly redder.

Finally, in Fig. 17 we show the old (10 Gyr) models for the same metallicities. In contrast to the younger models, in this case the flux increases with increasing wavelength in all the plotted SSP spectra. The sharp spectrum shape forced us to split this spectral range in four windows to be able to see the features, which are much stronger than in the youngest models. It is remarkable that some features, such as the Mg absorption around 2800 Å, become stronger with decreasing metallicity. This is however not the case for the neighbouring Mg absorption at 2852 Å. We discuss this issue in more detail in Section 4.3.

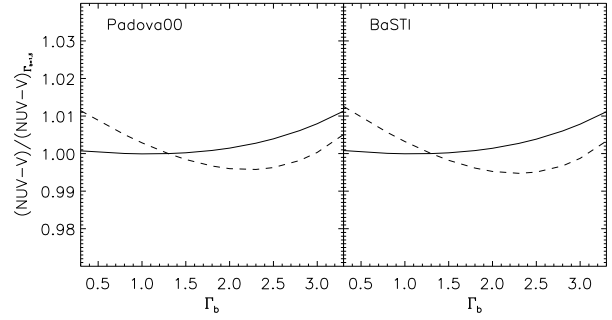


**Figure 14.** Dependence of the NUV-V colour on the bimodal IMF slope  $\Gamma_b$  for models of 10 Gyr (solid line) and 2 Gyr (dashed line) and solar metallicity. The obtained difference in colour with respect to the model with standard IMF slope, i.e.  $\Gamma_b = 1.3$ , is shown as a function of  $\Gamma_b$ , for models based on Padova00 (left panel) and BaSTI (right panel) isochrones.

### 4.3 Line-strengths

The UV model extension based on the NGSL allows us to work with line indices that are not covered by the SSP spectra computed with MILES. Table 3 lists the selected indices in this spectral range. Although our models allow us to optimize these indices for studying galaxy spectra, we adopt here the definitions from various sources, mostly from Fanelli et al. (1992). All the selected indices are defined by a feature bandpass and a pseudo-continuum at either side of the feature. In most cases the index definitions do not extend beyond  $\sim 200$  Å, from the bluest wavelength of the blue pseudocontinuum to the reddest wavelength of the red pseudocontinuum, with the notable exception of the Mg wide index, which covers 660 Å. The table also lists the main elements contributing to these features. We see that these lines are composed by different elements, being strongly blended in many cases. Note that the dominating elements might be at varying ionization stages (e.g., Mg II 2800 and Mg I 2852). Note also that the prominent Mg 2800 feature might be affected by chromospheric emission filling-in.

In Fig. 18 and Fig. 19 we show the behaviour of most of the UV line indices listed in Table 3 as a function of age for the SSP models computed with the BaSTI and Padova00 isochrones, respectively. The SSP spectra were smoothed to  $5$  Å (FWHM) ( $\sigma \sim 210$  km s $^{-1}$  at 3000 Å) to match the LIS-5.0 Å system defined in Vazdekis et al. (2010). Note that this is the nominal resolution of the models in the spectral range  $\lambda\lambda$  3060.8–3541.4 Å (see Table 1). The indices are ordered by increasing wavelength from the top-left to the bottom-right panels.

The strength of the reddest index, i.e. NH 3360, increases with increasing age and increasing metallicity, but shows a relatively more modest increase with age for ages larger than  $\sim 1$  Gyr. Such a behaviour is characteristic of many indices in the optical range (e.g. Vazdekis et al. 2010) and is related to the RGB phase. In the NIR range many indices tend to flatten even more (in some cases decrease) with increasing age (e.g. Röck et al. 2016). Note that for sub-solar metallicity models and ages above  $\sim 10$  Gyr the strength of the index tends to decrease due to the Horizontal-Branch bluing (more notorious in the BaSTI based models), as it happened to the NUV-V colour (see Section 4.1).

**Table 3.** UV Line-strength indices.

Index	Blue Passband	Index Passband	Red Passband	Contributions	Reference
BL 1719	1685 1705	1709 1729	1803 1823	N,S,Al	1,2
BL 1853	1803 1823	1838 1868	1885 1915	Al,Fe	1,2
Fe 2332	2285 2325	2333 2359	2432 2458	Fe,Co,Ni	1,3
Fe 2402	2285 2325	2382 2422	2432 2458	Fe,Co	1,2,3
BL 2538	2432 2458	2520 2556	2562 2588	Fe,Mg,Cr,Ni	1,2,3
Fe 2609	2562 2588	2596 2622	2647 2673	Fe,Mn	1,2,3
BL 2720	2647 2673	2713 2733	2762 2782	Fe,Cr	1,3
BL 2740	2647 2673	2736 2762	2762 2782	Fe,Cr	1,3
Mg 2800	2762 2782	2784 2814	2818 2838	Mg,Fe,Mn	1,2,3
Mg 2852	2818 2838	2839 2865	2906 2936	Mg,Fe,Cr	1,2,3
Mg wide	2470 2670	2670 2870	2930 3130	Mg,Fe,Cr	1,2,3
Fe 3000	2906 2936	2965 3025	3031 3051	Fe,Cr,Ni	1,2,3
BL 3096	3031 3051	3086 3106	3115 3155	Fe,Ni,Mg,Al	1,2,3
NH 3360	3320 3350	3350 3400	3415 3435	N,Mg,Fe,Ni	4
NH 3375	3342 3352	3350 3400	3415 3435	N,Ti,Ni	5
Mg 3334	3310 3320	3328 3340	3342 3355	Mg,O	5

- 1 Fanelli et al. (1990)  
 2 Maraston et al. (2009)  
 3 Chavez et al. (2007)  
 4 Davidge & Clark (1994)  
 5 Serven et al. (2011)

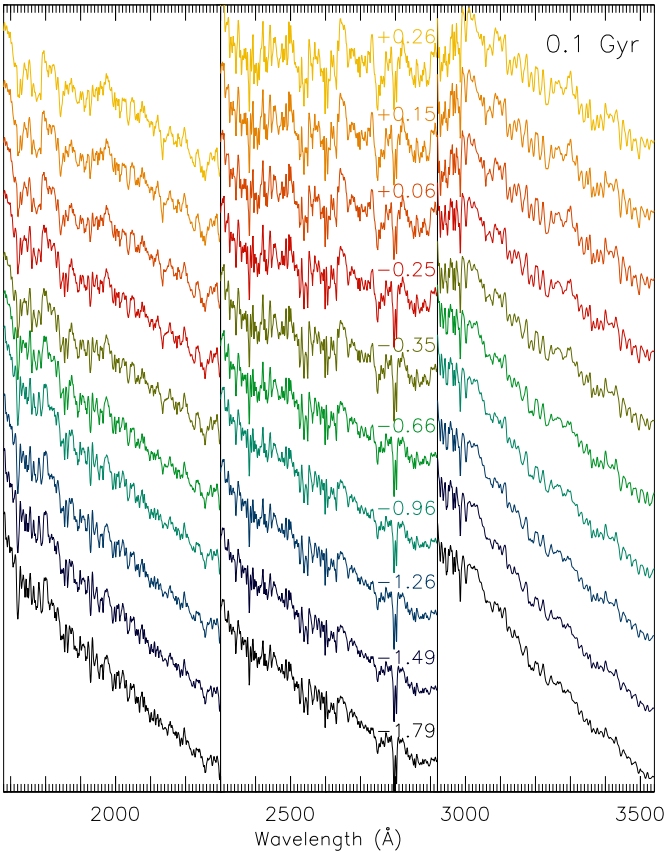


**Figure 15.** SSP spectra with age 0.1 Gyr and decreasing metallicity, from top to bottom as marked within the second window. All the models were computed with BaSTI isochrones and Kroupa Universal IMF. Note that the sharp spectrum shape of these models does not allow us to appreciate the details in the spectra if we do not split them in various windows.

The observed line-strength flattening of the NH 3360 index for ages above  $\sim 1$  Gyr is not seen for other indices with feature bandpasses redder than  $3000 \text{ \AA}$  (Mg 3334, BL 3096, and Fe 3000). This effect might be explained by the fast evolution of the temperature of the turnoff stars, which are more influential at these wavelengths (e.g. Chavez et al. 2007), whereas the RGB stars decrease their weight. The behaviour of these indices is therefore more similar to that of the NUV-V colour (see Section 4.1). This behaviour also applies to the Mg wide and Mg 2852 indices, which show a steady increase with increasing age.

Most of the indices centered within the range  $\lambda\lambda 2300 - 2900 \text{ \AA}$  show a very peculiar behaviour, as the index strengths of the more metal-rich stellar populations peak at intermediate ages. Moreover, for the Mg 2800, Fe 2402 and Fe 2332, the index values corresponding to the metal-poor SSPs can be larger than those of the metal-rich SSPs of very old ages. This result is in agreement with the models of Bruzual & Charlot (2003), based on theoretical stellar spectra, as shown by Daddi et al. (2005) (see their Fig. 2). This is a remarkable result, as our models predict a larger, e.g., Mg 2800 index values for the Milky-Way globular clusters with metallicities around  $[M/H] \sim -0.7$  than in giant elliptical galaxies. We discuss this issue in more detail in Section 6.3.1 and Section 6.3.2. It is worth noticing that the predicted strengths for the Mg 2800 index corresponding to the models with the youngest ages might be partially biased by interstellar absorption affecting some of the hot stars present in the NGSL (see Section 2.1). Note that in this respect the NGSL is not particularly different from the IUE stellar library employed by the models of Maraston et al. (2009). Therefore, judging from their Figure 10 where these authors show their predictions based on both the IUE stellar library and on theoretical spectra, we conclude that the net effect is smaller than  $\sim 1 \text{ \AA}$ . Furthermore, as in our case we decreased the relative weight of these stars when computing

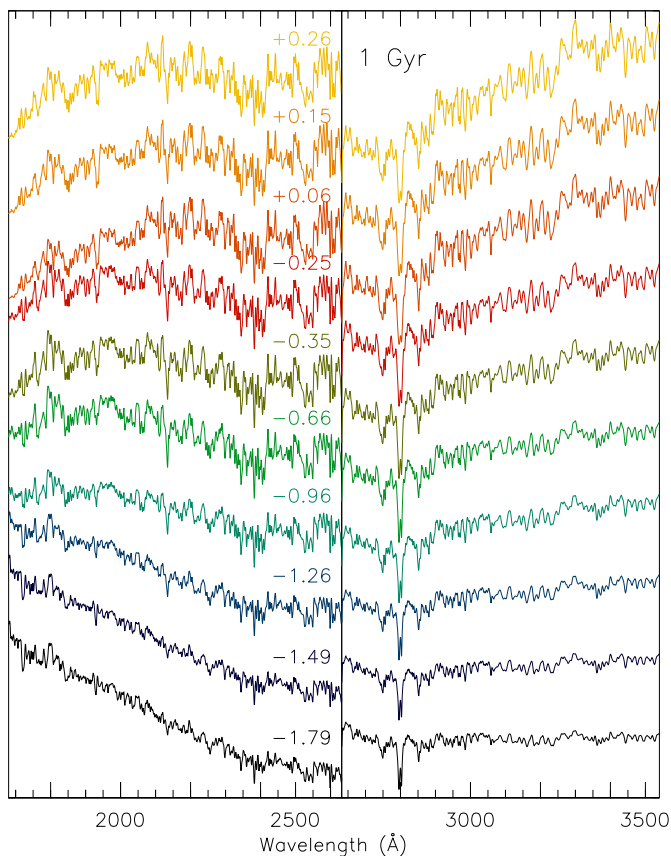


**Figure 16.** Same as in Fig. 15 but for models of 1 Gyr.

our SSP spectra (see Section 2.1), this effect is even smaller. Caveats should be taken into account by potential users of our models when applying them to this feature in such a young age regime.

Finally, the behaviour of the blended features BL 1719 and BL 1853, which fall within the bluest end of our spectral range coverage, resemble in part that of NH 3360. However for the age regime below  $\sim 1$  Gyr these indices decrease slightly with increasing age. This happens until reaching a certain age value, which is larger with decreasing metallicity.

In Fig. 20 we zoom in the spectral region around the Mg 2800 feature. The selected window covers the definition of the Mg wide index. Overplotted are various SSP models with 10 Gyr and different metallicities. Also plotted is a model of 2 Gyr and  $[M/H] = +0.06$  for which the strengths of the Mg 2800 and BL 2740 indices reach their maximum values. In contrast to these two indices, whose pseudocontinua and feature bandpasses are shown above the SSP spectra, the three indices shown below the spectra, namely Mg wide, BL 2720 and Mg 2852, increase their strength with increasing metallicity and increasing age. These spectra show that the Mg wide index measures a strong bump in the spectrum, which includes the two blends at 2720 Å and 2740 Å and the two Mg-dominated absorption features. As the metallicity and/or age increases the bump becomes more prominent and so the strength of this index. Similarly the two narrow indices BL 2720 and Mg 2852 show a very strong sensitivity to the metallicity and to the age. Furthermore, the sensitivity

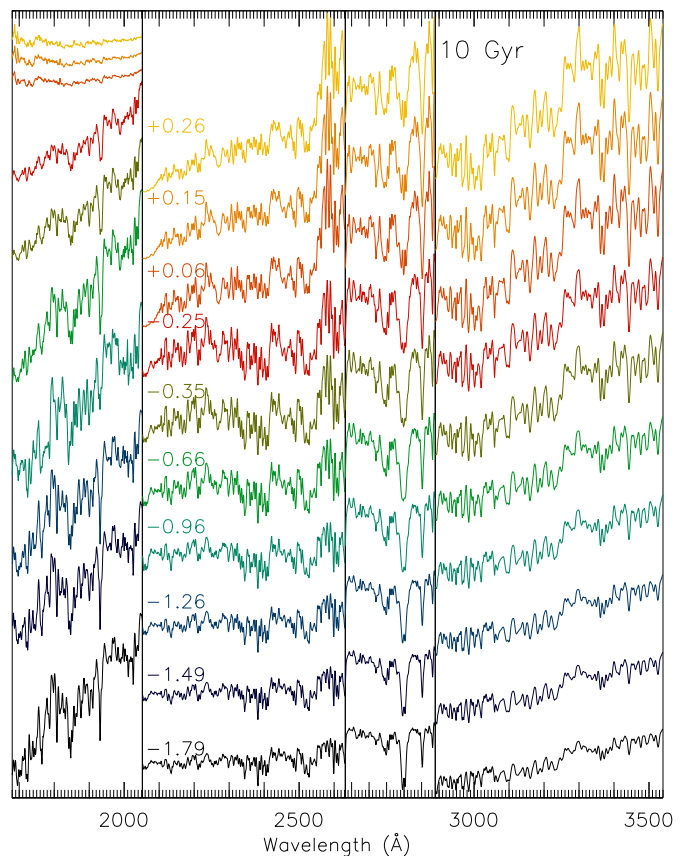


**Figure 17.** Same as in Fig. 15 and Fig. 16 but for models of 10 Gyr.

of the Mg 2852 index to these parameters is emphasized by the location of its red pseudocontinuum, redward  $\sim 2900$  Å, just on the top of a prominent flux jump, which is more pronounced for increasing metallicity/age with respect to the flux of its blue pseudocontinuum that sits within the bump. In contrast to Mg 2852 the Mg 2800 and BL 2740 indices do not show such sensitivity to the metallicity. As the two pseudocontinua are placed within the bump, a deeper bump leads to smaller fluxes, which plays against strengthening the measured index values. Fig. 20 shows that the behaviour of these indices as a function of metallicity and age does not solely depend on the depth of their absorption lines.

## 5 COMPARISON WITH OTHER MODELS

In this section we compare our models with other predictions found in the literature. Fig. 21 shows the behaviour of the NUV-V colour as a function of age for various SSP models. The figure shows the colours measured on our SSP spectra computed with the BaSTI and Padova00 isochrones, together with the colours of the models of Bruzual & Charlot (2003) for two different versions of the Padova isochrones (Bertelli et al. 1994; Girardi et al. 2000) and those of the models of Maraston (2005). For the latter models, we also show a version that makes use of a high resolution theoretical library (UVBLUE: Rodríguez-Merino et al. 2005) to obtain the NUV magnitudes for ages smaller than 1 Gyr and



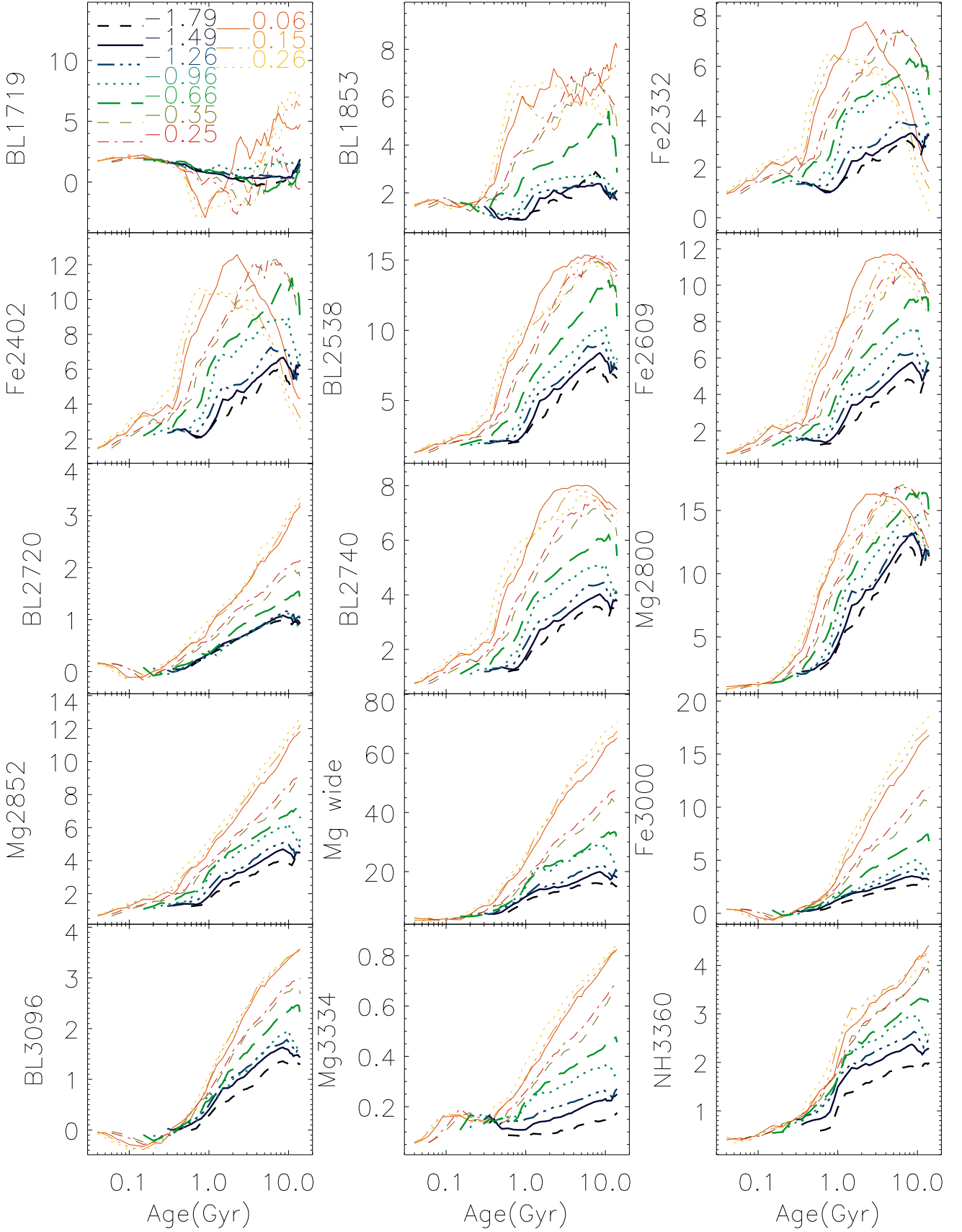


**Figure 18.** Behaviour of the UV line-strengths as a function of age and metallicity as quoted in the first panel. The SSP spectra, which were computed with the BaSTI isochrones adopting a Kroupa Universal IMF, were smoothed to 5 Å (FWHM) ( $\sigma \sim 210 \text{ km s}^{-1}$  at 3000 Å) to match the LIS-5.0 Å system defined in [Vazdekis et al. \(2010\)](#).

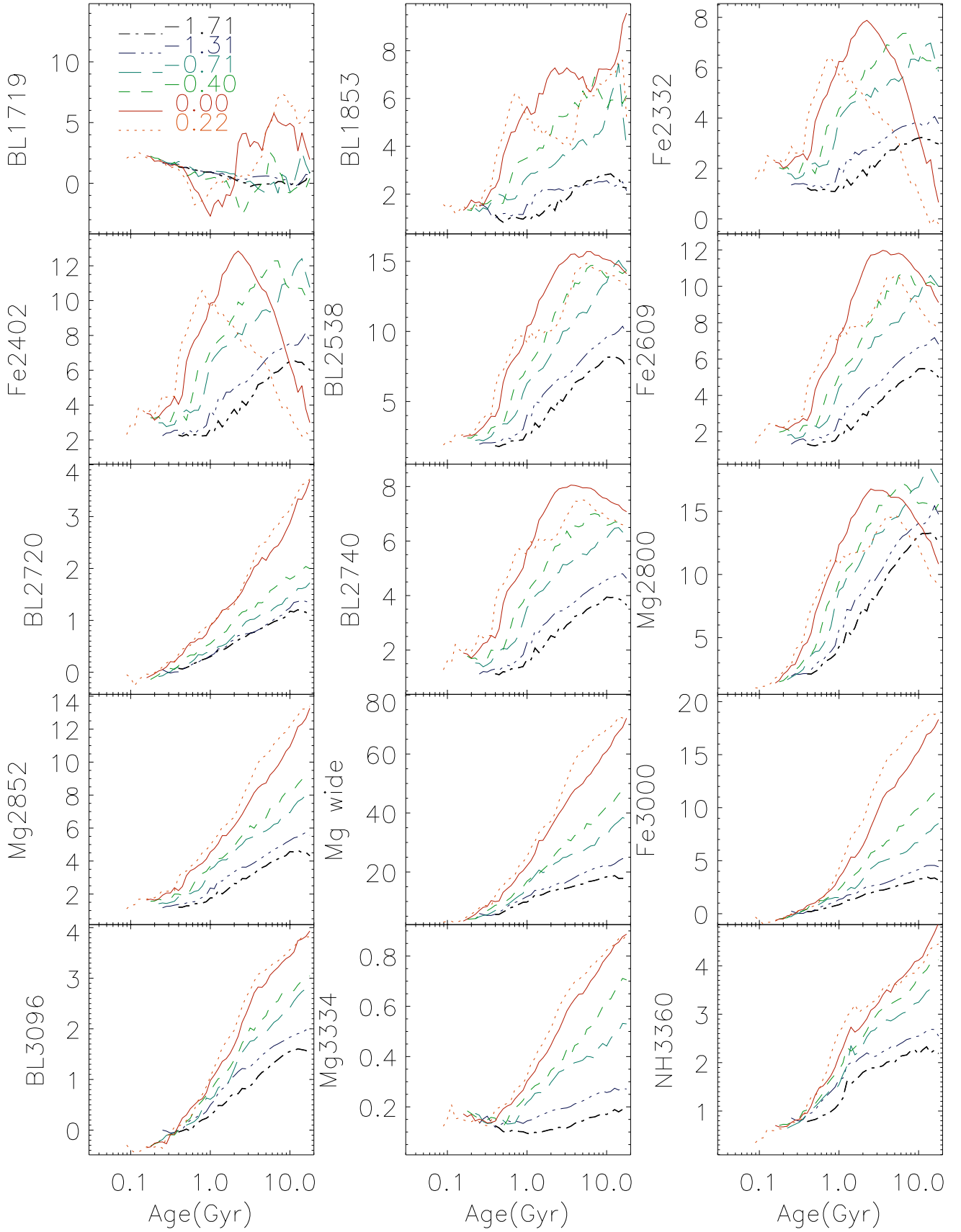


**Figure 19.** Same as Fig. 18, but for models computed with the Padova00 isochrones.

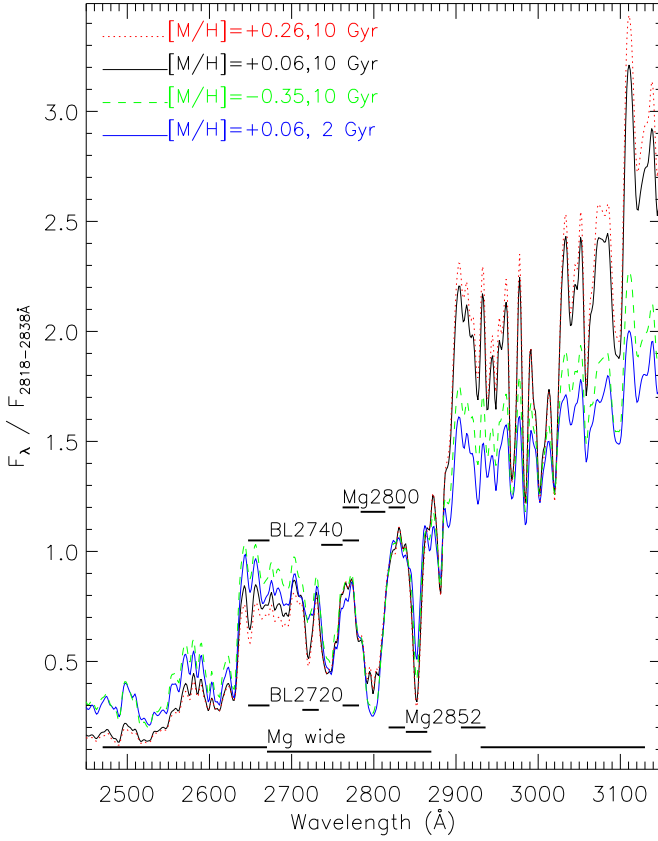


**Figure 20.** Spectral region around the Mg2800 feature with a number of SSP spectra of various ages and metallicities, as quoted within the panel, overplotted. All the spectra were normalized at the red pseudocontinuum of the Mg2800 index. The feature and pseudocontinua bandpasses corresponding to various indices in this spectral region are placed at a relatively slightly lower and higher flux level, respectively. The strengths of the indices marked above the spectra (i.e., BL2740 and Mg2800) peak at ages around  $\sim 2$  Gyr for metal-rich stellar populations, in contrast to the ones marked below the spectra. See for details Figs. 18 and 19 and the text.

solar metallicity. In all cases the models have solar metallicity. The comparison between our models, which are virtually similar for all the plotted ages, strongly suggests that the differences, mostly in the turnoff, have a minor secondary effect on the derived NUV magnitude. In comparison to the other authors our predictions provide the reddest colours for the oldest stellar populations and the bluest ones for the youngest stellar populations. Overall, we obtain a good agreement with the Maraston (2005) models for the whole age range shown in the figure. The young models of Maraston that are based on the UVBLUE theoretical library provide the worst agreement with our predictions. However the most significant disagreement is found when comparing either version of the Bruzual & Charlot (2003) for the oldest stellar populations. Their colours are around 1 magnitude bluer than all the other models shown here. This discrepancy can be attributed to the implementation of planetary nebulae spectra in the Bruzual & Charlot (2003) models, which make their SSP spectra particularly bluer at shorter wavelengths (private communication by G. Bruzual).

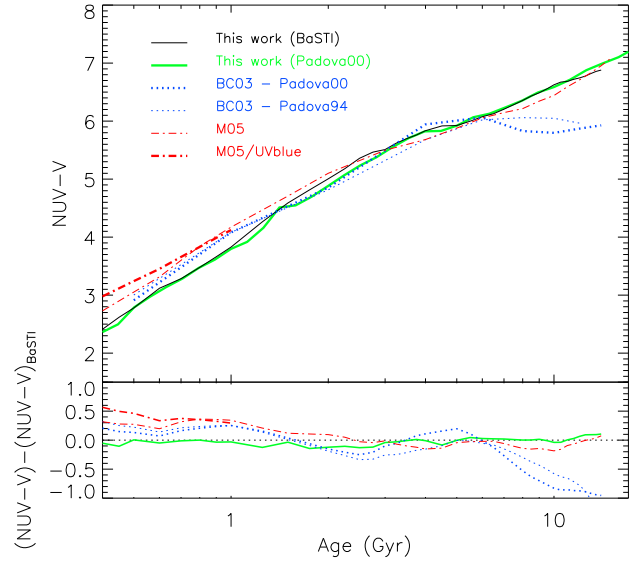


**Figure 21.** Comparison of NUV-V colour predictions from different authors, for solar metallicity SSPs and Kroupa Universal IMF. Black thin and green thick solid lines indicate our models, based on BaSTI and Padova00 isochrones, respectively. The blue lines represent the Bruzual & Charlot (2003), based on Bertelli et al. (1994) (thin dotted) and Girardi et al. (2000) (thick dotted) isochrones, and the red thin dot-dashed line represents the Maraston (2005) models. The thick red dot-dashed line shows a version of the latter models for ages smaller than 1 Gyr, where the NUV magnitude is computed with the UVBLUE theoretical stellar spectral library (Rodríguez-Merino et al. 2005). The lower panel shows the residual colours with respect to our BaSTI-based models.

In Fig. 22 we compare our SSP spectra with those of Bruzual & Charlot (2003) based on the IUE stellar library for various representative ages, namely 0.5, 2 and 10 Gyr. Overall the models are in agreement for the young and the intermediate age regimes, although there is a residual in the colour. The main difference is found for the models of 10 Gyr, as expected from the results obtained in Fig. 21. This discrepancy is more notorious at the bluest wavelengths, where the effects of the planetary nebulae spectra implemented in the Bruzual & Charlot (2003) models are larger.

## 6 APPLICATIONS

### 6.1 Colours

In order to assess the quality of our models, we compare the predictions for broad-band colours with data from globular clusters and nearby galaxies.

#### 6.1.1 Globular clusters

In Fig. 23 we show the integrated GALEX colours of the Galactic globular clusters from Dalessandro et al. (2012). The integrated magnitudes are measured from the surface brightness profile fitting method, that for most of the clusters agrees well with the aperture photometry method. The three clusters showing large discrepancies among the two

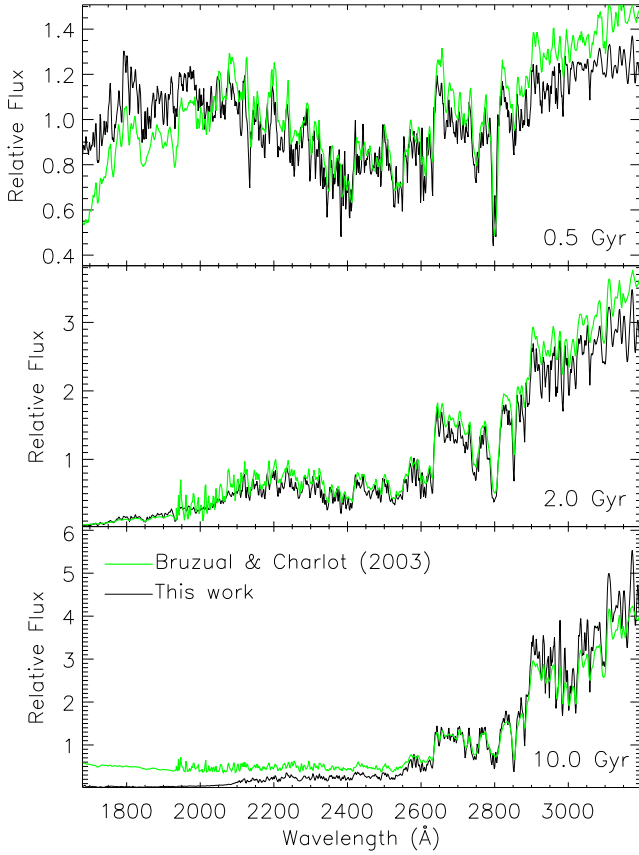


**Figure 22.** Comparison of various SSP spectra (black thin line) of varying ages (0.5, 2 and 10 Gyr from the top to the bottom panel, respectively) with those of Bruzual & Charlot (2003) (green thick line). All the models have solar metallicity and are computed adopting a Kroupa Universal IMF.

methods are shown as open circles in Fig. 23. Our models are shown for ages ranging from 8 to 14 Gyr and Kroupa Universal IMF. The Padova-based models show a fair agreement with data for nearly solar metallicity, but they appear too red in comparison to the metal-poor clusters. In the case of BaSTI-based models, the match with metal-poor clusters slightly improves. Note that due to the differences in the core He-burning phase (see Section 2), the metal-poor BaSTI-based models become bluer at old ages (see Fig. 13). Thus the oldest SSP (14 Gyr) is the one providing the best-fit to the data. Note also that at metallicity below  $-1.7$  our models are not safe and the comparison with data should be taken with caution.

To understand whether the HB morphology can have an impact on the integrated colours, we colour-code the clusters according to their HBR parameter (from Harris 2010). Clusters with blue and red morphology segregate in the high and low metallicity part of the diagram, respectively. For the clusters with  $[\text{Fe}/\text{H}] = -1.3$ , there is a hint suggesting that our models match better the redder HB morphologies, but, given the dispersion of the data, we cannot conclude that there is clear dependence of the NUV-V colour on the HBR parameter<sup>4</sup>.

<sup>4</sup> We have also looked for the Blue Stragglers (BS) determination

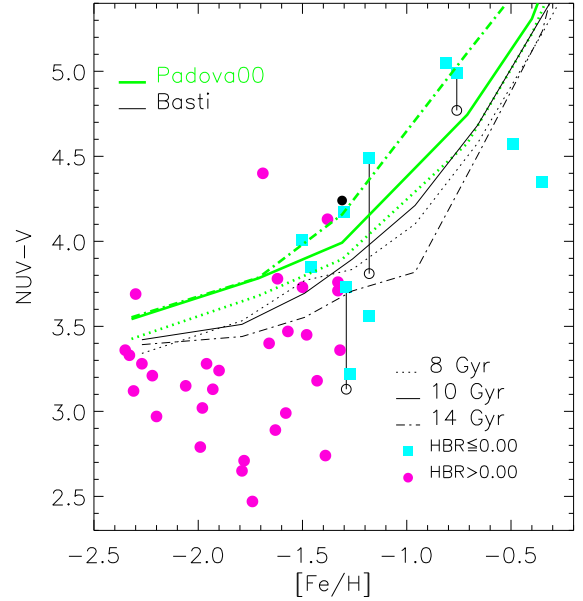


**Figure 23.** Dependence of the integrated NUV-V colour on metallicity for Galactic globular clusters. Symbols represent the GALEX data from Dalessandro et al. (2012). Magenta circles (cyan squares) represent data with blue (red) horizontal branch morphology, according to the HBR parameter from Harris (2010). Open circles represent the integrated colours measured from aperture photometry for the three clusters with large deviation from the surface profile fitting method. Overplotted are our model predictions based on the Padova00 (thick green lines) and BaSTI isochrones (thin black lines) for three SSP ages, as indicated. Old SSP models based on BaSTI provide a reasonably good fit to the data for metallicities above  $[\text{Fe}/\text{H}] = -1.5$  dex.

### 6.1.2 Galaxies

In Fig. 24 we compare our model predictions with data from nearby galaxies with GALEX observations, taken from Donas et al. (2007). To compute the synthetic colours, our models have been redshifted to  $z = 0.01$ , i.e. the median redshift of the observational sample. Both the ultraviolet and the optical colour (B-V) are given in the AB system and the observational data are corrected for Galactic extinction. In Fig. 24 we show the comparison with SSP models. Our models at subsolar and very low metallicity fit the galaxies with blue and intermediate colours. However the old models of solar and supersolar metallicity are too red to cover the redder, more massive, subsample of galaxies.

This mismatch cannot be attributed to the effects of the IMF, which is claimed to be bottom-heavy for such massive objects (La Barbera et al. 2013; Spiniello et al. 2014). These blue colours show little sensitivity to this parameter as shown in Fig. 14. It can be also argued that our NGSL based models follow the chemical evolution pattern of the solar neighborhood, being scaled-solar around the solar metallic-

in this sample of clusters and found 25 clusters with BS determination from Moretti, De Angeli & Piotto (2008) but no clear impact of the presence of BS on the colours is observed

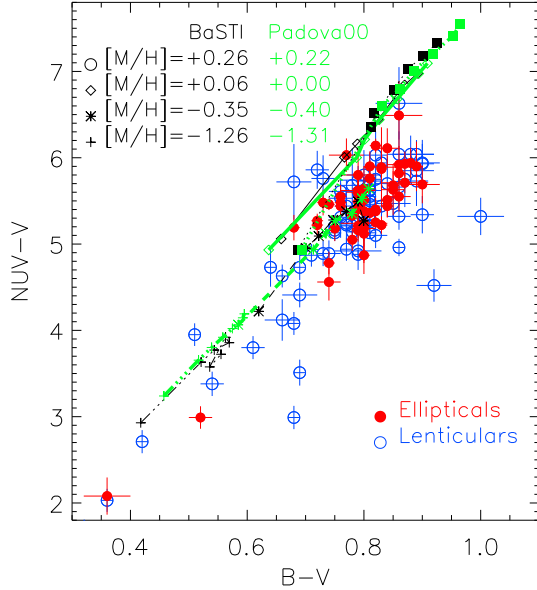


**Figure 24.** NUV–V vs. B–V colour-colour diagram for the nearby galaxy sample of Donas et al. (2007). The colours, which are given in AB magnitudes, are shown for galaxies classified as ellipticals (red solid circles) and lenticulars (blue open circles). Overplotted are our model predictions for SSP models based on Padova00 (green thick lines) and BaSTI (black thin lines) isochrones, for a Kroupa Universal IMF and different metallicities, as indicated by different line-types and quoted within the panel. The lines join SSP models of the same metallicity and ages ranging from 2 to 14 Gyr, from the bottom-left to the top-right. The plotted ages are 2, 5, 6.3, 8, 10, 12.5 and 14 Gyr for the predictions based on the Padova00 isochrones and 2, 5, 6, 8, 10, 12 and 14 Gyr for the models based on BaSTI isochrones. The model colours have been obtained after redshifting the SSP spectra to  $z = 0.01$ , i.e. the median redshift of the galaxy sample.

ity regime, whereas massive galaxies are nevertheless known to be [Mg/Fe]-enhanced (Worthey, Faber & González 1992). Therefore self-consistent SSP spectra with varying [Mg/Fe] ratios in this spectral range are required to test this possibility. In fact, we showed that such models improve the fits of the optical colours of these galaxies (Ricciardelli et al. 2012; Vazdekis et al. 2015). Although we are unable to show whether a better agreement is reached, we note that any solution should also match the line-strengths in this spectral range as we will show in Section 6.3.2. Finally, it might be also considered that the UV upturn phenomenon (e.g., Code & Welch 1979; Burstein et al. 1988), which affects the FUV spectral range of a fraction of these galaxies (e.g., Kaviraj et al. 2007; Yi et al. 2011), is also affecting the colours discussed here (e.g., Ponder et al. 1998). We have identified a number of well known galaxies showing the UV upturn (e.g., NGC 4552, one of the strongest UV upturn passive galaxies in the nearby Universe) as well as UV-weak galaxies (e.g., M 32). Although, for clarity, we do not mark them in Fig. 24, we find that these galaxies do not deviate significantly from the region where most galaxies are located. Specifically, the identified UV upturn galaxies do not prefer

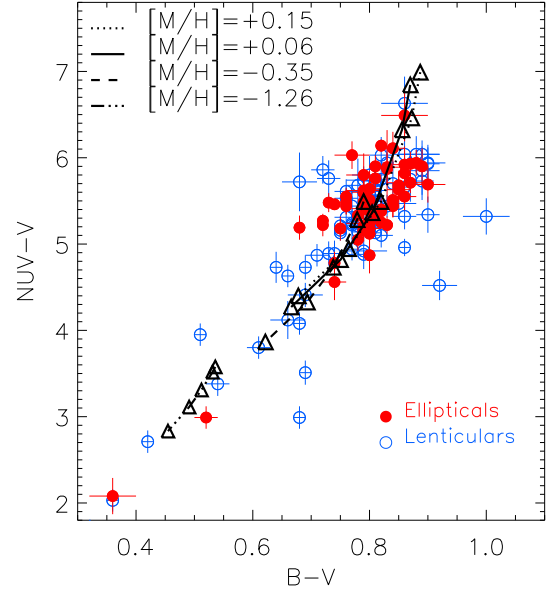


**Figure 25.** The same galaxy sample as in Fig. 24 is plotted here. Overplotted are model predictions (open triangles) for different metallicities obtained by combining two SSPs (based on BaSTI and adopting a Kroupa Universal IMF), one old with age 12 Gyr and the other young with 0.5 Gyr. The young component has varying mass fraction, namely 0, 0.1, 0.5, 1 and 2% from top to bottom, respectively.

the locus of the galaxy branch that cannot be matched by the SSP models alone.

In Fig. 25, we show the effect of an extended star formation history on this colour-colour diagram. We consider two burst models, where on top of the main burst with age 12 Gyr we add another burst of 0.5 Gyr, with varying mass fractions, namely 0, 0.1, 0.5, 1 and 2%. These combinations are made for varying metallicities from  $[\text{Fe}/\text{H}] = +0.15$  down to  $[\text{Fe}/\text{H}] = -1.26$ , as quoted within the figure. The addition of the young burst contributing with less than 1% to the mass in the solar and supersolar regime is very effective at bluening the colours by  $\sim 1$  mag in the NUV–V and by  $\sim 0.05$  in the B–V, thus bringing the models in better agreement with data. We also note that there is a bunch of galaxies with red B–V colour, likely the most massive ones, which are not properly matched by such combination of models. For this reason we plot in Fig. 26 other models where we combine an old component of 12 Gyr with varying fractions, from 0 to 2%, of a young component of varying age, namely 0.1, 0.5 and 1 Gyr. Both components, i.e. the old and the young, have the same metallicity  $[\text{Fe}/\text{H}] = +0.15$ , as this metallicity might be representative for the most massive galaxies as derived from detailed spectroscopic studies (e.g., La Barbera et al. 2013). We see that most of the galaxies, including those not matched by the SSP models in Fig. 24 and the combined models in Fig. 25, are now well reproduced by a varying fraction/age of the young component. We find that the best model combinations include young bursts in proportions that range from 0.1% of 0.1 Gyr to 2% of 1 Gyr, thus explaining the observed scatter in the galaxy distribution. These results are in very good agreement with previ-

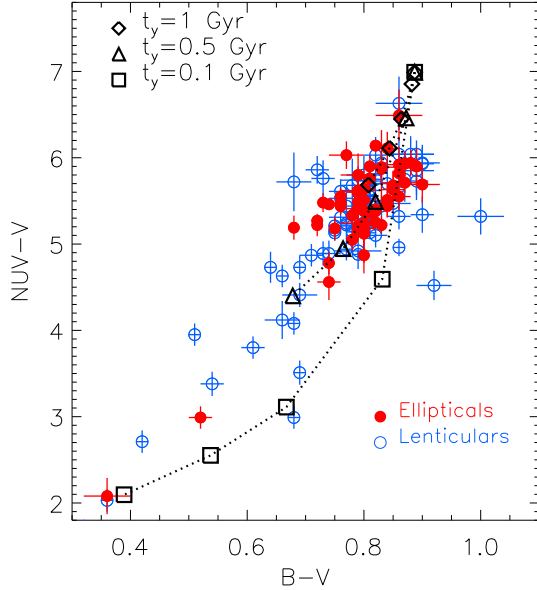


**Figure 26.** The same galaxy sample as in Fig. 24 and Fig. 25. Here we overplot combined models with metallicity  $[\text{Fe}/\text{H}] = +0.15$ , composed of an old SSP of 12 Gyr with varying mass fractions of a young component of 0.1 Gyr (open squares), 0.5 Gyr (open triangles) and 1 Gyr (open diamonds). The plotted fractions are 0, 0.1, 0.5, 1 and 2%, from top to bottom, respectively.

**Table 4.** SSP-equivalent ages and metallicities of a sample of ETGs with varying mass derived from full spectrum-fitting.

Galaxy	$\sigma$ (Km s $^{-1}$ ) <sup>a</sup>	Age (Gyr)	Metallicity (dex)
NGC 221	83	3.4 $\pm$ 0.1	+0.07 $\pm$ 0.01
NGC 3377	142	9.0 $\pm$ 0.5	-0.07 $\pm$ 0.04
NGC 6703	191	3.6 $\pm$ 0.5	+0.13 $\pm$ 0.05
NGC 3379	228	10.0 $\pm$ 0.3	-0.24 $\pm$ 0.02
NGC 1700	253	6.2 $\pm$ 0.4	-0.11 $\pm$ 0.03
NGC 4472	310	8.5 $\pm$ 4.1	+0.00 $\pm$ 0.31

<sup>a</sup> Taken from Toloba et al. (2009)

ously reported fractions and ages for the young components (e.g., Yi et al. 2011).

## 6.2 Spectra

In this section we apply full spectrum-fitting to a number of well selected ETGs from the sample of Toloba et al. (2009). The galaxies cover a wide mass range (velocity dispersion between 80 km s $^{-1}$  and 350 km s $^{-1}$ ) and have varying SSP-equivalent ages, as estimated from the optical spectral range. Although the wavelength coverage of the data ranges from 3150 Å to 4040 Å, here we focus on fitting the spectral region blueward the MILES range, i.e.  $\lambda\lambda$  3150–3500 Å. This allows us to show to what extent our results agree with those obtained in the optical range.

We use ULYSS<sup>5</sup>(Koleva et al. 2009), which is a full spec-

trum fitting package that performs  $\chi^2$ -fit between the observed spectrum and a linear combination of models. In this case we reconstruct the observations as SSPs convolved with the line-of-sight velocity dispersion (LOSVD) of the data, multiplied by a polynomial. We employ an interpolated grid of SSP spectra computed with Kroupa universal IMF. We injected the line spread function of the observations into the models to match their resolution and we used multiplicative polynomial of a degree 8 to minimise the mismatch between the high order changes in the observational flux (due to extinction and instrument) and the models. To fit the LOSVD of the galaxies with the lowest velocity dispersion (NGC 221 and NGC 3377) we smoothed them with a gaussian kernel of 150 km s $^{-1}$ . Finally, we used the automatic kappa-sigma clipping algorithm in ULYSS for the outliers.

In Fig. 27 we show the fits obtained for six galaxies, namely, NGC 221, NGC 1700, NGC 3377, NGC 3379, NGC 4472 and NGC 6703. The galaxies have been ordered according to increasing velocity dispersion from top to bottom. Galaxies for which the fits indicate very old stellar populations are plotted on the right panels, whereas their relatively younger counterparts are shown in the left panels. The obtained age and metallicity values are listed in Table 4. Our results for NGC 221 (M32) match those obtained by Sánchez-Blázquez et al. (2006b) on the basis of optical line-strength measurements. Similar results are also obtained by Vazdekis & Arimoto 1999; Worthey 2004; Rose et al. 2005). We also discuss the NUV indices of this galaxy in Section 6.3.2). The age that we obtain for NGC 3377 is larger than the value reported by Sánchez-Blázquez et al. (2006b) (5 Gyr), although it is similar to their age estimate based on spectral synthesis technique (9 Gyr). The age obtained for NGC 6703 is smaller than that of Sánchez-Blázquez et al. (2006b) (5.5 Gyr). For NGC 3379 these authors obtain a somewhat smaller age value (8 Gyr). The age obtained for NGC 1700 is in good agreement with Sánchez-Blázquez et al. (2006b). The results for this galaxy also agree with the detailed study performed by Kleineberg, Sánchez-Blázquez & Vazdekis (2011). In this work it is shown that this galaxy has a counterrotating, kinematically decoupled, core that is markedly younger than the main body of the galaxy. Finally we obtain for the cD galaxy in Virgo, NGC 4472, a good agreement with Sánchez-Blázquez et al. (2006b) (9.5 Gyr).

It is remarkable that the fits of such a narrow wavelength range in the NUV provide us with age values that are so similar to those obtained from detailed line-strength studies in the optical range. We therefore conclude that for these ETGs the dominant populations in this spectral window are not significantly different from those contributing in the visible.

In Fig. 28 we show the ULYSS fit obtained for M32 in the spectral range covering the Mg features at  $\sim$  2800 Å. We used for this purpose the spectrum observed with the IUE and presented in the catalog of McQuade, Calzetti & Kinney (1995) and Storchi-Bergmann, Kinney & Challis (1995)<sup>6</sup>. We find a solution that is  $\sim$  1 Gyr younger than that obtained in the redder wavelength range covered by Fig. 27 or in the opti-

<sup>5</sup> [ulyss.univ-lyon1.fr](http://ulyss.univ-lyon1.fr)

<sup>6</sup> [http://www.stsci.edu/ftp/catalogs/nearby\\_gal/sed.html](http://www.stsci.edu/ftp/catalogs/nearby_gal/sed.html)

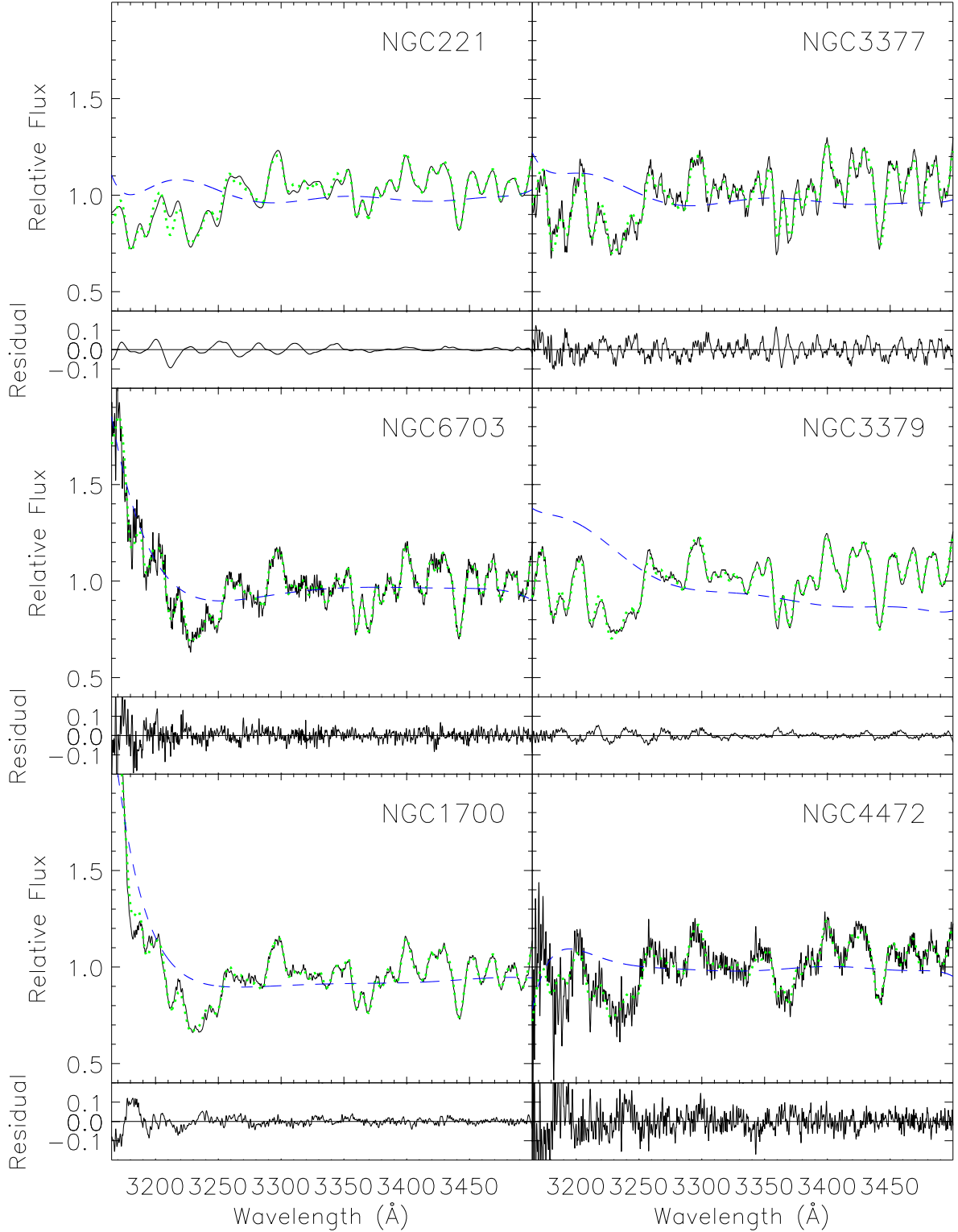


**Figure 27.** ULySS full spectrum-fits of a representative sample of galaxy spectra (quoted within the panels) of Toloba et al. (2009). In the upper panel for each galaxy we plot the observed spectrum in black and the best fitted model in thick dotted light green. The multiplicative polynomial employed in the fitting is shown in dashed blue. In the lower panel we plot the residuals (model-observation) with the same scale used for the spectra. We organized these plots such that the left panels correspond to galaxies for which we obtained relatively young ages in comparison to the ones in the right, which are old. The galaxies increase their velocity dispersion from top to bottom. The ages and metallicities of the best fitting models are listed in Table 4. In the text we discuss how these estimates compare to those from the literature that are based on detailed line-strength studies with high quality optical spectra.

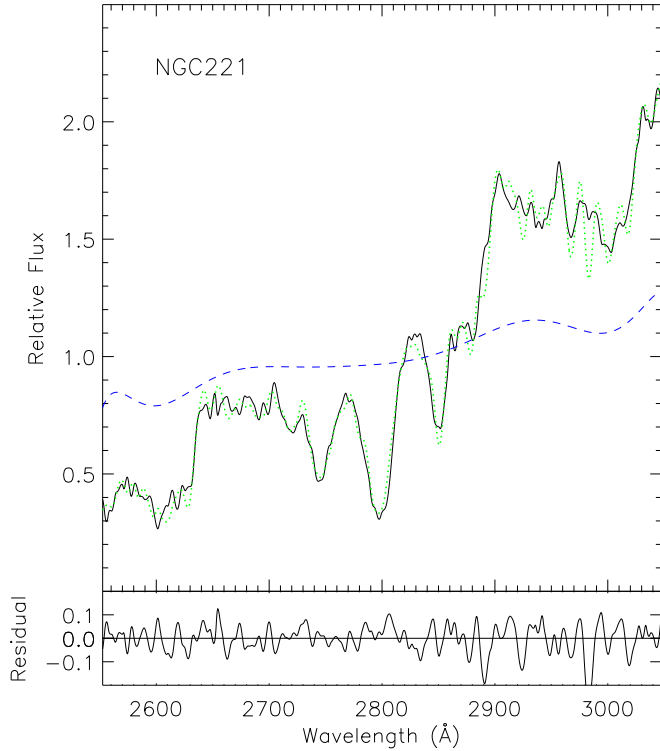


**Figure 28.** The upper panel shows the ULYSS fit of M32 in the spectral region around the Mg features at  $\sim 2800 \text{ \AA}$ . This spectrum, observed with the IUE, from the catalog of [McQuade, Calzetti & Kinney \(1995\)](#) and [Storchi-Bergmann, Kinney & Challis \(1995\)](#), is shown in black. Overplotted in thick dotted light green is a model with age 2.3 Gyr and metallicity  $[M/H] = +0.11$ . All the plotted spectra have a resolution of  $\sigma = 270 \text{ km s}^{-1}$ . The multiplicative polynomial employed in the fitting is shown in dashed blue. In the lower panel we plot the residuals (model-observation) with the same scale used for the spectrum.

cal range. Although this spectrum, which is among the ones with the highest S/N in the catalog, has a rather modest quality for this type of analysis, this result suggests a somewhat more extended SFH than just an SSP of  $\sim 3$  Gyr. Note that this is expected as the obtained solution is biased toward a younger age when fitting bluer wavelengths.

### 6.3 Line-strengths

#### 6.3.1 Stellar clusters

To assess the reliability of our new models we compare the predicted line-strengths with those of globular clusters, for which Colour-Magnitude Diagram (CMD) derived ages and metallicities are available. These objects can be considered to a good approximation a single-burst like stellar population, which is characterized by a single age and a single metallicity. Therefore they can be treated as real SSP templates to test our model SSPs, with the caveats that many clusters seem to be composed by more than just one stellar component (e.g., [Meylan 2003](#); [Cassisi & Salaris](#)

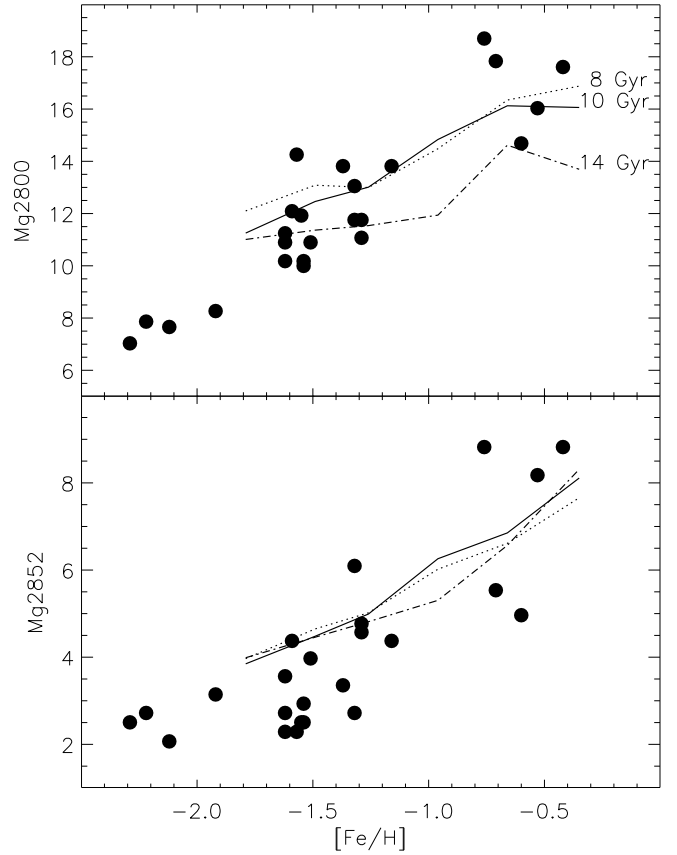


**Figure 29.** Mg 2800 (upper panel) and Mg 2852 (lower panel) UV indices of the globular clusters of the Milky Way, observed with the IUE and measured by [Rose & Deng \(1998\)](#). The metallicities tabulated in the [Harris \(1996\)](#) catalog are adopted. Overplotted are our SSP models, based on the BaSTI isochrones and adopting a Kroupa Universal IMF, smoothed to match the IUE resolution. The predicted indices for three ages, namely 8, 10 and 14 Gyr, are represented with different line types, as quoted within the upper panel, as a function of metallicity.

[2013](#)) and that stochastic effects may be noticed in their integrated spectra (e.g., [Cerviño et al. 2002](#)). We also note that the claimed difference in age among the various stellar components within a cluster is certainly negligible in comparison to their old ages, while the difference in the abundance ratios of individual elements might be more notorious in some line indices (e.g., [Piotto et al. 2012](#); [Gratton, Carretta & Bragaglia 2012](#)).

We use the line-strength measurements of [Rose & Deng \(1998\)](#) for the Milky Way clusters, which were observed with the IUE. No errorbars are provided by these authors. Fig. 29 shows the observed values for the Mg 2800 and Mg 2852 indices, as well as those of our SSP models once smoothed to match the IUE resolution. We show the predictions for three age values (8, 10 and 14 Gyr), which are representative of the globular cluster ages, as a function of metallicity. The metallicities of the clusters are taken from [Harris \(1996\)](#). Overall we see that our models match reasonably well the two indices. For the Mg 2800 index there is a hint of a slightly younger age for the metal-rich clusters, although this is not conclusive given the large scatter of the data. However most of the metal-poor clusters tend to be bluer than our pre-



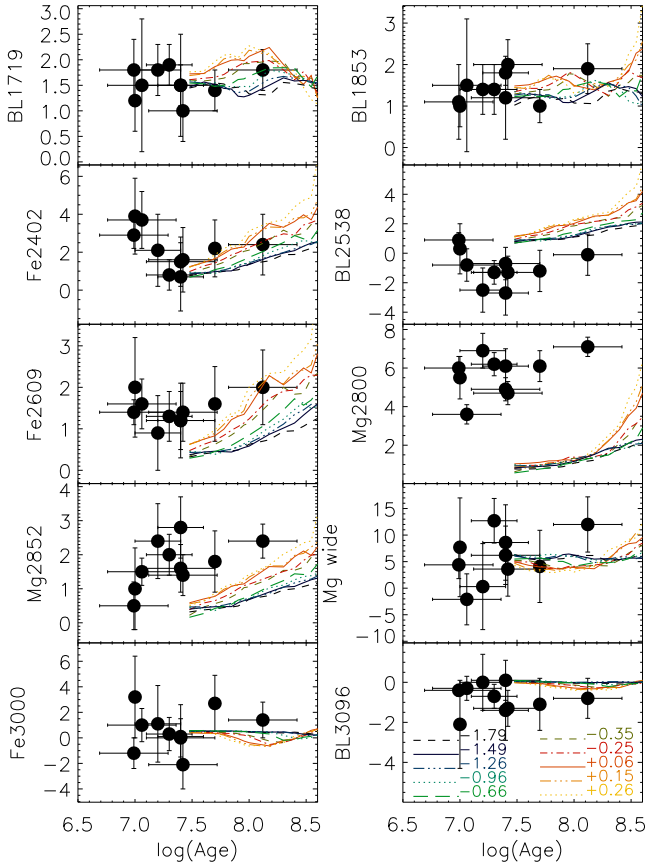


**Figure 30.** UV line indices for the LMC clusters plotted against their CMD-derived ages, all taken from [Maraston et al. \(2009\)](#). Our young BaSTI-based SSP models with Kroupa Universal IMF, smoothed to match the IUE resolution, are plotted for different metallicities with different line types and colours, as quoted within the last panel.

dictions, similarly to the results obtained for the NUV–V colour, which can be explained by a bluer HB morphology for these clusters than is adopted by the models.

To validate our youngest models we employ observations of the Large Magellanic Cloud (LMC) stellar clusters. In Fig. 30 we compare our models to the line-strength measurements of [Maraston et al. \(2009\)](#) using IUE data from [Cassatella, Barbero & Geyer \(1987\)](#), which are plotted as a function of the CMD ages derived by various authors ([Elson & Fall 1988](#); [Elson 1991](#); [Dirsch et al. 2000](#); [de Grijs et al. 2002](#)). A comparison of this figure with figures 9 and 10 of [Maraston et al. \(2009\)](#) shows a good agreement between our predictions and their models based on the IUE stellar spectra. The main differences are generally found for ages above 100 Myr. Also, for the BL 3096 index our model values are about  $0.5 \text{ \AA}$  smaller than theirs, in better agreement with the data. Finally we also note that a worse agreement is reached when compared to their fully theoretical model predictions.

Most of the LMC clusters plotted in Fig. 30 are younger than our models with the lowest age, i.e. 30 Myr ( $\log(\text{Age}) = 7.48$ ). However we see that an extrapolation of the model lines toward younger ages match most of the plotted in-

dications within their errorbars. This is the case for the BL 1719, BL 1853, Fe 2402, Mg wide, Fe 3000 and BL 3096 indices. Our models provide slightly larger values for the BL 2538 and slightly smaller index strengths for Fe 2609 and Mg 2852 indices. However a strong discrepancy is found for the Mg 2800 index, for which our models provide around  $5 \text{ \AA}$  smaller values. Note that this is remarkable, given the good agreement found for the Milky Way old clusters, as shown in Fig. 29 and our good match to the broadband Mg wide index. A similar discrepancy is obtained when these clusters are compared to the [Maraston et al. \(2009\)](#) models (see their Figure 10). These authors attribute this strong Mg absorption to contamination by interstellar lines from warm neutral interstellar medium of the LMC, which affects this Mg region. We refer the interested reader to [Maraston et al. \(2009\)](#) for a more extended discussion on this discrepancy.

### 6.3.2 Early-Type galaxies

To compare our predicted line-strengths to index measurements of ETGs we selected the sample of six elliptical galaxies of [Ponder et al. \(1998\)](#) (NGC 3605, 3608, 5018, 5831, 6127 and 7619). The galaxy spectra were obtained with the Faint Object Spectrograph on the HST covering the UV spectral range at a resolution of  $8 \text{ \AA}$ , with  $S/N > 20$  and flux accuracy of  $\sim 5\%$ . Fig. 31 shows these galaxies (solid circles), with their errorbars, for 10 UV line-strength indices. We assume for these galaxies the mean luminosity-weighted ages derived from the optical range based on line-strength studies. We adopt the ages of [Sánchez-Blázquez et al. \(2006b\)](#) for NGC 3605, 3608 and 6127 (3.25, 8.43 and 8.45 Gyr, respectively), [Leonardi & Worthey \(2000\)](#) for NGC 5018 (2.8 Gyr), with an errorbar adjusted to match the younger age value provided by [Terlevich & Forbes \(2002\)](#) (i.e. 1.5 Gyr), [Vazdekis et al. \(2004\)](#) for NGC 5831 (5.9 Gyr), and [González-Delgado et al. \(2015\)](#) for NGC 7619 (9.77 Gyr). In addition we also include the index values provided by [Ponder et al. \(1998\)](#) for M32, obtained with the IUE by [Buson, Bertola & Burstein \(1990\)](#). No errorbars are provided for this galaxy. We adopt the central age value obtained by [Rose et al. \(2005\)](#) (3 Gyr). The galaxies cover a rather wide range in velocity dispersion, from  $\sigma \sim 80 \text{ km s}^{-1}$  (M32) to  $\sim 350 \text{ km s}^{-1}$  (NGC 7619). Note that we did not attempt to homogenize these age estimates, which may vary among authors employing different age-dating line-strength based methods and models. We selected studies based on spectra of very high quality, which suffices for the purposes of this comparison. Roughly, the age of these galaxies increases with increasing  $\sigma$ , with the notable exception of NGC 5018 ( $280 \text{ km s}^{-1}$ ), our youngest object, which is considered a remnant merger ([Fort et al. 1986](#)).

It is worth quoting that these old galaxies show Mg 2800 values significantly smaller than those shown by the MW globular clusters as seen in Fig. 29 (regardless a relatively minor correction due to the varying velocity dispersion), in good agreement with the expected trend with varying metallicity from our model predictions. However we see that the observed indices for these massive galaxies are smaller than those predicted by our metal-rich SSP models. In fact, in contrast to M32, whose measured indices are well matched by a solar metallicity SSP with age in good agreement

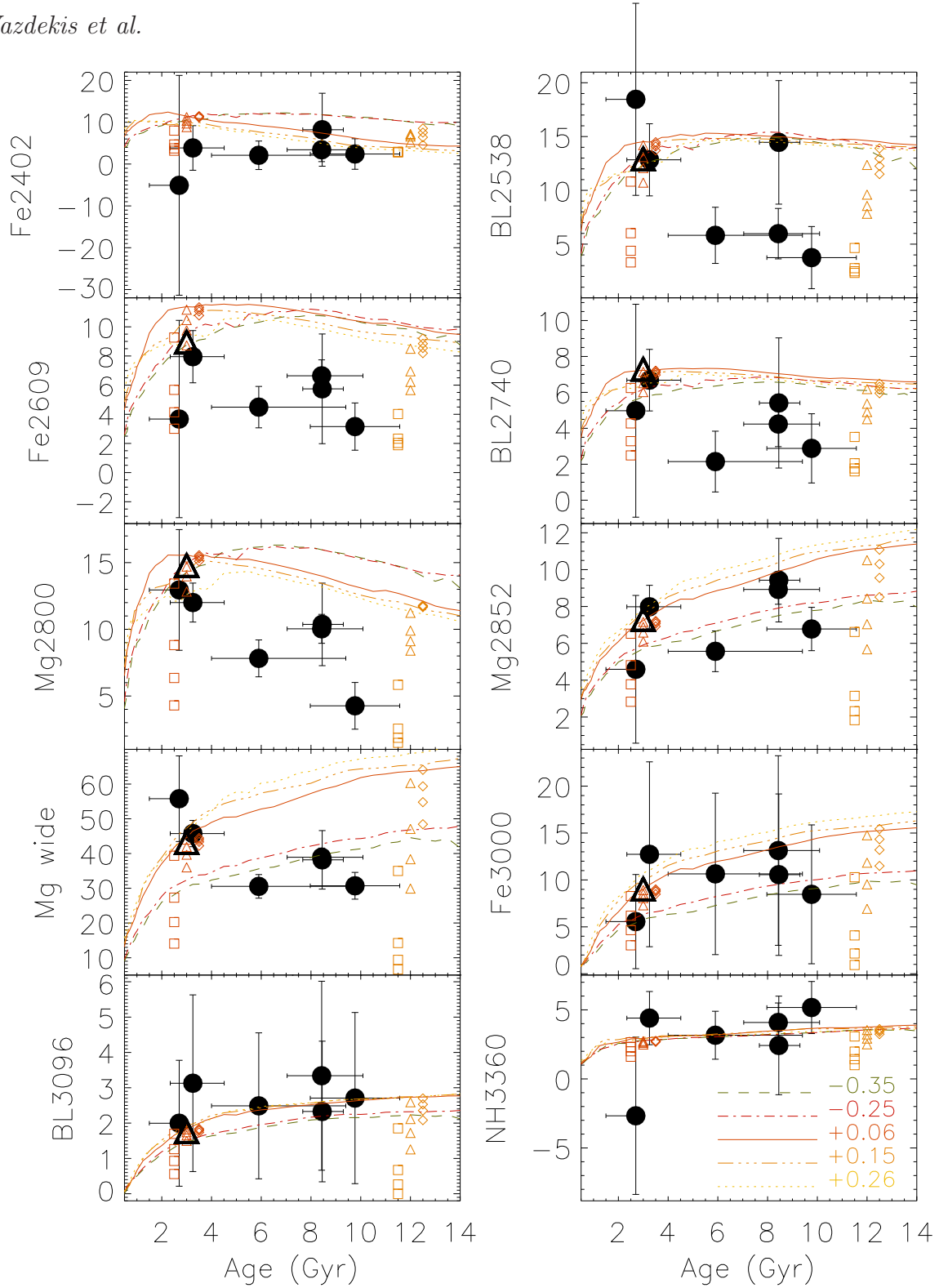


**Figure 31.** UV line-strengths of elliptical galaxies in the Ponder et al. (1998) sample. The galaxies, with varying velocity dispersion, were observed with FOS at the HST, and are shown as filled circles. M 32, which was observed with the IUE, is plotted as an open triangle. These galaxies display a rather wide coverage in mean luminosity-weighted age as estimated from the optical spectral range (see the text for references). Our SSP model predictions for different metallicities are shown in coloured lines and varying types as quoted within the last panel. Both galaxy and model line-strengths are shown at a resolution of  $300 \text{ km s}^{-1}$ . We also show the line-strengths resulting from combining a 12 Gyr model with a varying fraction of a young model with age 0.1 Gyr (open orange squares), 0.5 Gyr (open orange triangles) and 1 Gyr (open orange diamonds), all with supersolar metallicity  $[\text{Fe}/\text{H}] = +0.15$ , which can be considered representative for the oldest (massive) galaxies. The mass fraction of the young component is increased by 0.1, 0.5, 1 and 2% from top to bottom, resulting in an increasing departure from the reference SSP value at 12 Gyr, which is located on the model line (three dots - dashed) corresponding to this metallicity at 12 Gyr. These symbols were separated arbitrarily from the reference age value for visibility. Similarly, we also plot the combination of a model of age 3 Gyr with young models with similar ages and fractions, all with metallicity  $[\text{Fe}/\text{H}] = +0.06$ . We use similar symbols, this time in red and placed at 3 Gyr. The larger the young mass fraction the larger the deviation from the reference SSP value located on the solid red line at this age.

with its literature determination ( $\sim 3$  Gyr), this is not the case for various of the old massive galaxies. Specifically our metal-rich SSP models predict larger values for the BL 2538, Fe 2609, BL 2740, Mg 2800, Mg 2852, Mg wide and Fe 3000 indices.

A bottom-heavy IMF, as recently claimed for massive early-type galaxies (e.g., La Barbera et al. 2013; Spiniello et al. 2014), decreases the Mg 2800 index by only  $\sim 1 \text{ \AA}$  for an SSP with a bimodal IMF with slope 2.8, which is clearly insufficient for matching the observed index values of these massive objects. Small index variations are also obtained for the other indices, confirming the very small sensitivity of this spectral range to the IMF, as already found for the colours (see Fig. 14).

We also investigate whether the existence of an old metal-poor contribution in addition to a dominant metal-rich population (e.g., Vazdekis et al. 1997; Maraston & Thomas 2000) is capable of matching the observed index values. Note however that the observed values deviate in different proportions and sometimes in different direction to the expected index variation due to a decrease in metallicity. Therefore, if we construct a model that is composed of two old SSPs, one metal-rich and the other one metal-poor, we could in principle match the Mg wide index. On the contrary we are unable to match simultaneously the Mg 2800 index, for which we will predict a larger value in comparison to a metal-rich SSP. It can be argued that the Mg 2800 could be affected by chromospheric emission filling-in, thus making the index smaller. However such a model combination cannot match for example the Fe 2609 and Fe 3000 pair of indices simultaneously either. Therefore we can safely rule out such a combined model for matching the UV line-strength indices of these massive galaxies.

As an alternative scenario we also study the impact of a young component on these indices. Such a scenario has been proposed in the literature to explain for example the scatter of the Balmer absorption lines in the optical range (e.g., Leonardi & Rose 1996; Trager et al. 2000). For this purpose we plot in Fig. 31 the line-strength values resulting from combining an model with age 12 Gyr with a young model with age 0.1, 0.5 and 1 Gyr, all with metallicity  $[\text{Fe}/\text{H}] = +0.15$ , which is representative for these massive galaxies. The mass fraction of the young component is varied from 0.1 to 2%, which is reflected by an increasing deviation from the reference SSP value, which is located on the model line of the same metallicity at 12 Gyr. We see that all the indices are matched for the model combination including 0.1% of a young component of age 0.1 Gyr. Also, a reasonably good match is achieved when we include 0.5–1% of a population with age 0.5 Gyr. This set of UV indices is not only allowing us to detect young contributions but also to constrain their ages. In fact it can be seen that when using a component of 1 Gyr there are indices that cannot be matched such as BL 2538, BL 2609, BL 2740 or Mg 2800. Such a combination can be therefore ruled out. Note that what really matters is the age of this component, as the impact of varying the fraction is much smaller. Therefore these indices allow us to break the burst-age, burst-strength degeneracy (Leonardi & Rose 1996). Note that the effects of these young contributions is far less notorious for the reddest indices, i.e. as we approach to the optical range. Also the effects are relatively small for our bluest index Fe 2402,

in this case because these young populations still show as large index values as the old component.

It is worth noticing that our purpose with these model combinations is not to properly fit these data, but to illustrate the abilities of this set of UV indices to constrain the presence of such young stellar components. The ages and fractions obtained with these indices are in good agreement with those inferred from the colours as shown by Fig. 26. In principle, we also could explain the observed index scatter shown by these old galaxies by a varying age, and to a lesser extent by a varying fraction, of these young components.

It is remarkable the very good agreement achieved for M32, with just an SSP of age similar to that corresponding to the mean luminosity-weighted age derived from the optical range. The center of this galaxy is known to be a factor of  $\sim 2$  younger than at  $1 r_e$  (e.g., Worthey 2004; Rose et al. 2005). Such a relatively young mean luminosity-weighted age in the optical range suggests the presence of a population with age smaller than the determined mean optical age value. It is therefore expected that such a population is largely dominating the light of this galaxy in the UV range. In fact, the younger the mean optical age the more relevant is the contribution of this relatively young population, and far smaller that of the old component. In Fig. 31 we also show what impact the presence of even younger populations has on a dominating population with age 3 Gyr and metallicity  $[\text{Fe}/\text{H}] = +0.06$ . We use the same ages and fractions employed to illustrate the effects on a dominant old population. We see that the impact of these younger contributions is notoriously less influential on the indices than it was the case for older galaxies. We note specifically that the ages and fractions of the young stellar components that are required to match the UV indices for the old galaxies (i.e. 0.1% of 0.1 Gyr and 0.5 – 1.0% of 0.5 Gyr) have little impact on the indices of the dominating population of 3 Gyr. To create a noticeable effect, larger fractions and younger contributions are needed, as illustrated by the combination with a 0.1 Gyr and mass fractions 0.5, 1 and 2%. Overall we also see that these fractions tend to provide a slightly better agreement for the other young galaxies in this sample. To summarize, the population with age  $\sim 3$  Gyr completely dominates the integrated light of these galaxies in the UV. Note, however, that our ULySS fit to this galaxy in the spectral range around the Mg features at  $\sim 2800 \text{ \AA}$  suggests a somewhat more extended SFH as we estimate a slightly younger age. A more quantitative study is beyond the scope of this paper but will be addressed elsewhere. However these results illustrate the ability of the UV to detect and constrain the contribution of young populations that do not show up so clearly in redder spectral ranges, particularly for the old galaxies.

## 7 SUMMARY AND CONCLUSIONS

We employ the New Generation Stellar Library (NGSL), which was observed with the Hubble Space Telescope, to extend our stellar population synthesis models to the UV spectral range. The stellar parameters coverage of this library, which were determined in Koleva & Vazdekis (2012) and transformed to match those of the MILES library (Cenarro et al. 2007a) on which our models in the

optical range are based, allowed us to compute single-age, single-metallicity stellar population (SSP) spectra in the metallicity range  $-1.79 < [M/H] < +0.26$  and ages larger than 30 Myr. These models represent a significant improvement over earlier studies based on the IUE stellar library (Wu et al. 1983; Fanelli et al. 1992) as the NGSL feeding our models has a better stellar parameter coverage, resolution and S/N. We provide a quantitative assessment of the quality of these models within these ranges. The models were computed with two sets of isochrones, Padova00 (Girardi et al. 2000) and BaSTI (Pietrinferni et al. 2004, 2006) as extended in Vazdekis et al. (2015). These isochrones were transformed to the observational plane with metallicity dependent colour-temperature relations from extensive photometric empirical (rather than theoretical) stellar libraries (mainly Alonso et al. 1996, 1999). The models were computed for a suite of IMF types: Kroupa Universal and Revised (Kroupa 2001), (Chabrier 2001) and the single-power law (unimodal) and double-power law low-mass tapered (bimodal) IMFs of (Vazdekis et al. 1996). We also varied the slope of the unimodal IMF and the high-mass end ( $M > 0.6 M_{\odot}$ ) slope of the bimodal IMF.

The computed SSP spectra in the UV range cover  $\lambda\lambda$  1680.2–3541.4 Å, with constant resolution FWHM = 3 Å for  $\lambda < 3060.8$  Å and FWHM = 5 Å for  $3060.8 < \lambda < 3541.4$  Å. These SSP spectra were joined to those computed with MILES (Sánchez-Blázquez et al. 2006) in the optical range, as well as with our models for redder wavelengths, all computed with the same code and prescriptions and employing empirical stellar libraries, i.e. Indo-US (Valdes et al. 2004), CAT (Cenarro et al. 2001a,b) and IRTF (Cushing et al. 2005; Raynier et al. 2009), to obtain self-consistent E-MILES SSP spectra covering the range  $\lambda\lambda$  1680–50000 Å at moderately high resolution (FWHM = 2.5 Å from 3541.4 Å to 8950.4 Å and  $\sigma = 60 \text{ km s}^{-1}$  for larger wavelengths). As a sanity check, we compared the U-B colour measured on the E-MILES spectra to those based on the photometric predictions (using the same photometric libraries employed to transform the isochrones to the observational plane), reaching a good agreement (typically within 0.02 mag). The reliability of the E-MILES SSP models depend on the spectral range. We refer the reader to the specific papers, listed in Table 1, of the models joined here for assessing their quality.

We focus on studying the behaviour of the colours, spectra and line-strength indices of the SSP spectra in the UV range. The NUV-V colour shows a steady increase with increasing age (and metallicity), in contrast to the more flattened behaviour shown by the optical colours for ages above  $\sim 1$  Gyr. Note that such a flattening is far more pronounced for the near-IR colours. We show that the effects of the IMF on the NUV-V colour is almost negligible. We also study the behaviour of the UV line-strength indices as a function of relevant stellar population parameters. We find that some UV indices increase with increasing age and metallicity, as it happens for most of the metallicity indicators in the optical range. However, there are other indices within the range 2300–2800 Å, such as Mg at 2800 Å, which peak at intermediate ages in the range 1–6 Gyr for metal-rich stellar populations, whereas for lower metallicities they keep strengthening with increasing age. The indices within the spectral

range 3000–3500 Å show a larger sensitivity to the age in comparison to their counterparts in the optical range.

We compare our models to other models in the literature that employ the IUE (Fanelli et al. 1992), i.e. an alternative space-based stellar library with lower spectral resolution. Our NUV-V colour is in reasonably good agreement with the models of Maraston (2005). It also agrees with those of Bruzual & Charlot (2003), except for ages above  $\sim 10$  Gyr, which are  $\sim 1$  mag bluer than ours. This is attributed to the fact that these models incorporate some spectra of planetary nebulae that shine in the shortest wavelengths of the spectral range covered by our SSP spectra. The UV line-strengths of our SSP models with ages smaller than  $\sim 0.5$  Gyr are in good agreement with those shown by Maraston et al. (2009). For older ages, the peculiar behaviour shown by the Mg 2800 index as a function of age for metal-rich stellar populations, is also seen in the models of Bruzual & Charlot (2003), as shown in Daddi et al. (2005).

Our models match reasonably well the integrated NUV-V colours of the Milky-Way globular clusters of higher metallicities as well as a fraction of the metal-poor clusters. However for other metal-poor clusters our colours are redder by  $\sim 0.5$  mag. Our models provide good fits to the Mg 2800 and Mg 2852 indices of the Milky Way globular clusters. Moreover, most of the UV line-strengths of the LMC clusters, with ages typically smaller than 100 Myr, are reasonably well fitted by our models. However, a strong discrepancy is found with respect to the Mg 2800 measured in these clusters, confirming the result previously reported by Maraston et al. (2009).

The comparison of our models with UV data of ETGs, shows the unprecedented power of this spectral range to constrain the contributions from young stellar populations to the total light, particularly for the oldest objects. We find that both, the NUV-V colour and the UV line-strengths, of massive ETGs reveal the presence of young stellar components on top of the old stellar populations, with ages in the range 0.1 – 0.5 Gyr that represent 0.1 – 0.5% in mass fraction. The remarkable variety in the behaviour of the different UV line indices as a function of age, has allowed us to rule out stellar contributions with ages around  $\sim 1$  Gyr. Our age/fraction estimates for these young components are in agreement with previous results obtained in this spectral range (e.g., Yi et al. 2011). We also find that the age of these young components could be more important than their relative contributions. Variations in the ages, and in the relative fractions, of these younger components might potentially fill in the scatter observed for the NUV-V colour and the UV line-strengths of ETGs. It is worth noticing that such tiny contributions do not affect significantly the age estimates obtained from the age indicators in the optical range, such as  $H\beta$  (these young components will make these old galaxies to look 1 – 2 Gyr younger if measured with this Balmer index).

For M 32 we obtain very good fits using an SSP model of  $\sim 3$  Gyr (and solar metallicity). This is attributed to the fact that this galaxy is claimed to be dominated by a stellar population of such age, which outshines these small contributions from the young components that we infer for the older, more massive, ETGs.

We also performed full-spectrum fits in the spectral window  $\lambda\lambda$  3200–3500, using UlySS (Koleva et al. 2009), for a

representative set of ETGs with varying mass and ages. The resulting SSP age and metallicity estimates are in very good agreement with detailed line-strength studies performed in the optical range. Note that the results obtained for the most massive objects in our sample, i.e. the same ages as inferred from the optical range, do not contradict the ones that we obtained by fitting the UV line-strengths, as the indices that are able to constrain the presence of young contributions are found at bluer wavelengths ( $< 3000 \text{ \AA}$ ). Put in other words, the spectral range employed for our full-spectrum fits provides similar constraints as the optical range. However our fit of NGC 221 in the spectral region covering the Mg features around  $2800 \text{ \AA}$  suggests a more extended SF, rather than just a single  $\sim 3 \text{ Gyr}$  old dominating population.

The E-MILES models computed here provide new means for constraining the most likely Star Formation Histories experienced by massive galaxies. In particular the extremely wide spectral coverage of these models can be used to separate the various stellar populations contributing to the total light in the various wavelength ranges. The ample coverage in age, metallicity and IMF, allow us to study smaller galaxies and stellar clusters of varying ages. The UV range covered by these models will help to understand the evolution of these objects as seen at different redshift ranges. These models, which are aimed for interpreting incoming data from ground- and space-based observing facilities, can be retrieved from the MILES website <http://miles.iac.es>. The webpage also provides user-friendly tools for handling the model spectra for their use for the analysis of the data.

## ACKNOWLEDGMENTS

We are grateful to M. Beasley, J. Beckman, F. La Barbera and R. Peletier for very useful discussions and valuable suggestions. We thank G. Bruzual for providing us with various versions of his models in the UV spectral range and for interesting suggestions. We also thank E. Toloba for providing us with fully-reduced early-type galaxy spectra. We are grateful to the anonymous referee for valuable suggestions that helped us to improve the paper. This research has made an extensive use of the SIMBAD data base and VizieR catalogue access tool (both operated at CDS, Strasbourg, France), the NASA's Astrophysics Data System Article Service. This work has been supported by the grants AYA2013-48226-C3-1-P and AYA2013-48226-C3-2-P from the Spanish Ministry of Economy and Competitiveness (MINECO) and the Generalitat Valenciana under grant PROMETEOII/2014/069. E.R. acknowledges a Marie Heim-Vögtlin grant from the Swiss National Science Foundation.

## REFERENCES

Alexander, D. R., Ferguson, J. W., 1994, *ApJ*, 437, 879  
 Alonso, A., Arribas, S., Martínez-Roger, C., 1995, *A&A*, 297, 197  
 Alonso, A., Arribas, S., Martínez-Roger, C., 1996, *A&A*, 313, 873  
 Alonso, A., Arribas, S., Martínez-Roger, C., 1999, *A&AS*, 140, 261  
 Bertelli, G., Bressan, A., Chiosi, C., Fagotto, F., Nasi, E., 1994, *A&AS*, 106, 275

Bessell, M. S., Brett, J. M., Wood, P. R., Scholz, M., 1989, *A&AS*, 77, 1  
 Bessell, M. S., Brett, J. M., Scholz, M., Wood, P. R., 1991, *A&AS*, 89, 335  
 Bressan, A., Chiosi, C., Fagotto, F., 1994, *ApJS*, 94, 63  
 Bruzual, G., Charlot, S., 2003, *MNRAS*, 344, 1000  
 Burstein, D., Bertola, R., Buson, L. M., Faber, S. M., Lauer, T. R., 1988, *ApJ*, 328, 440  
 Buser, R., Kurucz, R. L., 1978, *A&A*, 70, 555  
 Buson, L. M., Bertola, F., Burstein, D., 1990, in *Windows on Galaxies*, eds. G. Fabbiano, J.S. Gallagher & A. Renzini (Boston: Kluwer), 51.  
 Carretero, C., Vazdekis, A., Beckman, J., Sánchez-Blázquez, P., Gorgas, J., 2004, *ApJ*, 609, L45  
 Cassatella, A., Barbero, J., Geyer, E. H., 1987, *ApJS*, 64, 83  
 Cassisi, S. & Salaris, M. 2013 "Old stellar populations: how to study the fossil record of galaxy formation", Wiley-VCH eds., Berlin  
 Cassisi, S., Salaris, M., Castelli, F., Pietrinferni, A., 2004, *ApJ*, 616, 498  
 Cassisi, S., Castellani, V., Ciarcelluti, P., Piotto, G., Zoccali, M., 2000, *MNRAS*, 315, 679  
 Cenarro, A. J., Cardiel, N., Gorgas, J., Peletier, R. F., Vazdekis, A., Prada, F., 2001a, *MNRAS*, 326, 959  
 Cenarro, A.J., Gorgas, J., Cardiel, N., Pedraz, S., Peletier, R. F., Vazdekis, A., 2001b, *MNRAS*, 326, 981  
 Cenarro, A. J., et al., 2007a, *MNRAS*, 374, 664  
 Cerviño, M., Valls-Gabaud, D., Luridiana, V., Mas-Hesse, J. M., 2002, *A&A*, 381, 51  
 Chabrier, G., 2001, *ApJ*, 554, 1274  
 Chavez, M., Bertone, E., Buzzoni, A., Franchini, M., Malagnini, M. L., Morossi, C., Rodriguez-Merino, L. H. 2007, *ApJ*, 647, 1046  
 Chung, C., Yoon, S.-J., Lee, S.-Y., Lee, Y.-W., 2013, *ApJS*, 204, 3  
 Cervantes, J. L., Vazdekis A., 2009, *MNRAS*, 392, 691  
 Cid Fernandes, R., Mateus, A., Sodré, L., Stasińska, G., Gomes, J. M., 2005, *MNRAS*, 358, 363  
 Cimatti, A., Daddi, E., Renzini, A., et al. 2004, *Nature*, 430, 184  
 Code, A. D., & Welch, G. A., 1979, *ApJ*, 228, 95  
 Coelho, P., Barbuy, B., Melendez, J., Schiavon, R., Castilho, B., 2005, *A&A*, 443, 735  
 Coelho, P., Bruzual, G., Charlot, S., Weiss, A., Barbuy, B., Ferguson, J. W., 2007, *MNRAS*, 382, 498  
 Conroy, C., Gunn, J. E., 2010, *ApJ*, 712, 833  
 Conroy C., van Dokkum P., 2012a, *ApJ*, 747, 69  
 Conroy, C., Graves, G., van Dokkum, P., 2014, *ApJ*, 780, 33  
 Cordier, D., Pietrinferni, A., Cassisi, S., Salaris, M., 2007, *AJ*, 133, 468  
 Cushing, M. C., Raynier, J. T., Vacca, W. D., 2005, *ApJ*, 623, 1115  
 Daddi, E., et al., 2005, *ApJ*, 626, 680  
 Dalessandro, E., Schiavon, R. P., Rood, R. T., Ferraro, F. R., Sohn, S. T., Lanzoni, B., O'Connell, R. W., 2012, *AJ*, 144, 126  
 Davidge, T. J., Clark, C. C., 1994, *AJ*, 107, 946  
 de Boer, K. S. 1985, *A&A*, 142, 321  
 de Grijs, R., Gilmore, G. F., Johnson, R. A., Mackey, A. D., 2002, *MNRAS*, 331, 245  
 de Mello, D. F., Daddi, E., Renzini, A., et al. 2004, *ApJ*, 608, L291  
 Dirsch, B., Richtler, T., Gieren, W. P., Hilker, M., 2000, *A&A*, 360, 133  
 Donas, J. et al., 2007, *ApJS*, 173, 597  
 Dorman, B., O'Connell, R. W., Rood, R. T., 1995, *ApJ*, 442, 105  
 Elson, R. A. W., 1991, *ApJS*, 76, 185  
 Elson, R. A. W., Fall, S. M., 1988, *AJ*, 96, 1383  
 Faber S. M., 1983, *Highlights Astron.*, 6, 165  
 Falcón-Barroso, J., Sánchez-Blázquez, P., Vazdekis, A., Riccia-

- rdelli, E., Cardiel, N., Cenarro, A. J., Gorgas, J., Peletier, R. F., 2011, *A&A*, 532, 95
- Fanelli, M. N. O., O’Connell, R. W., Burstein, D., Wu, C.-C., 1990, *ApJ*, 364, 272
- Fanelli, M. N. O., O’Connell, R. W., Burstein, D., Wu, C.-C., 1992, *ApJS*, 82, 197
- Fioc, M., Rocca-Volmerange, B., 1997, *A&A*, 326, 950
- Fitzpatrick, E. L., 1999, *PASP*, 111, 63
- Fluks, M. A., Plez, B., Thé, P. S., de Winter, D., Westerlund, B. E., Steenman, H. C., 1994, *A&AS*, 105, 311
- Fort, B. P., Prieur, J.-L., Carter, D., Meatheringham, S. J., Vigroux, L. 1986, *ApJ*, 306, 110
- Fritze-Von Alvensleben, U. A, Gerhard, O. E., 1994, *A&A*, 285, 751
- Fukugita, M., Shimasaku, K., Ichikawa, T., 1995, *PASP*, 107, 945
- Génova, R., Molaro, P., Vladilo, G., Beckman, J. E., 1990, *ApJ*, 355, 150
- Girardi, L., Bressan, A., Bertelli, G., Chiosi, C., 2000, *A&AS*, 141, 371
- González-Delgado, R., et al., 2015, *A&A*, 581, 103
- Gratton, R. G., Carretta, E., Bragaglia, A., 2012, *ARAA*, 20, 50
- Gregg, M. D., Silva, D., Rayner, J., et al. 2006, in *The 2005 HST Calibration Workshop: Hubble After the Transition to Two-Gyro Mode*, ed. A. M. Koekemoer, P. Goudfrooij, & L. L. Dressel, 209–215
- Harris, W. E., 1996, *AJ*, 112, 1487
- Harris, W. E., 2010, arXiv:1012.3224
- Hayes, D. S., 1985, in D. S. Hayes, L. E. Pasinetti, & A. G. D. Philip, eds. *Proc. IAU Symposium 111, Calibration of fundamental stellar quantities*. Dordrecht, Reidel, p., 225.
- Heap, S. R., Brown, T. M., Hubeny, I., et al. 1998, *ApJ*, 492, L131
- Heap, S. & Lindler, D. J. 2009, in *New Quests in Stellar Astrophysics. II. Ultraviolet Properties of Evolved Stellar Populations*, ed. M. Chávez Dagostino, E. Bertone, D. Rosa Gonzalez, & L. H. Rodriguez-Merino, 273–281
- Hernández-Pérez, F. & Bruzual, G. 2014, *MNRAS*, 444, 2571
- Jones, L. A., 1999, Ph.D. thesis, Univ. of North Carolina, Chapel Hill
- Kaviraj, S. et al., 2007, *ApJS*, 173, 619
- Kleineberg, K., Sánchez-Blázquez, Vazdekis, A., 2011, *ApJ*, 732, L33
- Kodama T., Arimoto N., 1997, *A&A*, 320, 41
- Koleva, M., Prugniel, P., Bouchard, A., Wu, Y., 2009, *A&A*, 501, 1269
- Koleva, M., Vazdekis, A., 2012, *A&A*, 538, 143
- Kroupa, P., 2001, *MNRAS*, 322, 231
- La Barbera, F., Ferreras, I., Vazdekis, A., de la Rosa, I. G., de Carvalho, R. R. Trevisan, M., Falcón-Barroso, J., Ricciardelli, E., 2013, *MNRAS*, 433, 3017
- Le Borgne, J.-F., Bruzual, G., Pelló, R., Lancon, A., Rocca-Volmerange, B., Sanahuja, B., Schaerer, D., Soubiran, C., Vílchez-Gómez, R., 2003, *A&A*, 402, 433
- Le Borgne, J.-F., Rocca-Volmerange, B., Prugniel, P., Lancon, A., Fioc, M., Soubiran, C., 2004, *A&A*, 425, 881
- Leitherer, C., et al., 1999, *ApJS*, 123, 3
- Lejeune, T., Cuisinier, F., Buser, R., 1997, *A&AS*, 125, 229
- Lejeune, T., Cuisinier, F., Buser, R., 1998, *A&AS*, 130, 65
- Leonardi, A., Rose, J. A., 1996, *AJ*, 111, 182
- Leonardi, A., Worthey, G., 2000, *ApJ*, 534, 650
- MacArthur, L. A., 2005, *ApJ*, 623, 795
- Maeder, A., Meynet, G., 2000, *A&A*, 361, 159
- Maraston, C., 1998, *MNRAS*, 300, 872
- Maraston, C., 2005, *MNRAS*, 362, 799
- Maraston, C., Colmenárez, L. N., Bender, R., Thomas, D., 2009, *A&A*, 493, 425
- Maraston C., Strömbäck G., 2011, *MNRAS*, 418, 2785
- Maraston C., Thomas D., 2000, *ApJ*, 541, 126
- McQuade, K., Calzetti, D., Kinney, A. L. 1995, *ApJS*, 97, 331
- Meneses-Goytia, S., Peletier, R., Trager, S., Vazdekis, A., 2015, *A&A*, 582, 97
- Meylan G., 2003, in "New Horizons in Globular Cluster Astronomy", ASP Conference Proceedings, eds. G. Piotto, G. Meylan, S. G. Djorgovski, M. Riello. Vol., 296, p.17
- Mignoli, M., Cimatti, A., Zamorani, G., et al., 2005, *A&A*, 437, 883
- Montes, M., Acosta-Pulido, J. A., Prieto, M. A., Fernández-Ontiveros, J. A., 2014, *MNRAS*, 442, 1350
- Moretti, A., De Angeli, F., Piotto, G., 2008, *A&A*, 483, 183
- Ocvirk, P., Pichon, C., Lancon, A., Thiébaud, E., 2006a, *MNRAS*, 365, 74
- Percival, S. M., Salaris, M., 2011, *MNRAS*, 412, 2445
- Pettini, M., Steidel, C. C., Adelberger, K. L., Dickinson, M., Gialavalisco, M., 2000, *ApJ*, 528, 96
- Pietrinferni, A., Cassisi, S., Salaris, M., Castelli, F., 2004, *ApJ*, 612, 168
- Pietrinferni, A., Cassisi, S., Salaris, M., Castelli, F., 2006, *ApJ*, 642, 797
- Pietrinferni, A., Cassisi, S., Salaris, M., Percival, S., Ferguson, J. W., 2013, *ApJ*, 697, 275
- Pietrinferni, A., Cassisi, S., Salaris, M., Hidalgo, S., 2013, *A&A*, 558, 46
- Piotto, G., Milone, A. P., Anderson, J., Bedin, L. R., Bellini, A., Cassisi, S., Marino, A. F., Aparicio, A., Nascimbeni, V., 2012, *ApJ*, 760, 39
- Ponder, J. M., Burstein, D., O’Connell, R. W., Rose, J. A., Frogel, J. A., Wu, C.-C., Crenshaw, D. M., Rieke, M. J., Tripicco, M., 1998, *AJ*, 116, 2297
- Popesso, P., Dickinson, M., Nonino, M., et al. 2009, *A&A*, 494, 443
- Prugniel, P., Soubiran, C., 2001, *A&A*, 369, 1048
- Raynier, J. T., Cushing, M. C., Vacca, W. D., 2009, *ApJS*, 185, 289
- Reimers, D., 1977, *A&A*, 57, 395
- Renzini, A., 2006, *ARAA*, 44, 141
- Ricciardelli, E., Vazdekis, A. Cenarro, A. J., Falcón-Barroso, J., 2012, *MNRAS*, 424, 172
- Röck, B., Vazdekis, A., Ricciardelli, E., Peletier, R. F., Knapen, J. H., Falcón-Barroso, J., 2016, *A&A*, 589, 73
- Röck, B., Vazdekis, A., Peletier, R. F., Knapen, J. H., Falcón-Barroso, J., 2015, *MNRAS*, 449, 2853
- Rodríguez-Merino, L. H., Chavez, M., Bertone, E., Buzzoni, A., 2005, *ApJ*, 626, 411
- Rose, J. A., 1984, *AJ*, 89, 1238
- Rose, J. A., 1985, *AJ*, 90, 1927
- Rose J. A., Deng, S., 1999, *AJ*, 117, 2213
- Rose, J. A., Arimoto, N., Caldwell, N., Schiavon, R. P., Vazdekis, A., Yamada, Y., 2005, *AJ*, 129, 712
- Salpeter, E. E., 1955, *ApJ*, 121, 161
- Sánchez-Blázquez, P., Gorgas, J., Cardiel, N., González, J. J., 2006b, *A&A*, 457, 809
- Sánchez-Blázquez, P., et al., 2006, *MNRAS*, 371, 703
- Schiavon, R. P., 2007, *ApJS*, 171, 146
- Schiavon R. P., Caldwell N., Rose J. A., 2004, *AJ*, 127, 1513
- Schiavon, R. P., Faber, S. M., Castilho, B. V., Rose, J. A., 2002, *ApJ*, 580, 850
- Serven, J., Worthey, G., Briley, M. M., 2005, *ApJ*, 627, 754
- Serven, J., Worthey, G., Toloba, E., Sánchez-Blázquez, P., 2011, *AJ*, 141, 184
- Smith, G. H., Burstein, D., Fanelli, M. N., O’Connell, R. W., Wu, C.-C., 1991, *AJ*, 101, 655
- Smith, R. J., Lucey, J. R., Carter, D., 2012, *MNRAS*, 421, 2982
- Spiniello, C., Trager, S., Koopmans, L. V. E., Conroy, C., 2014, *MNRAS*, 438, 1483
- Storchi-Bergmann, T., Kinney, A. L., Challis, P. 1995, *ApJS*, 98, 103
- Terlevich, A. I, Forbes, A. D., 2002, *MNRAS*, 330, 547

- Thomas, D., Maraston, C., Bender, R., 2003, MNRAS, 339, 897
- Tinsley, B. M., 1980, Fundam. Cosmic Phys., 5, 287
- Tojeiro, R., Percival, W. J., Heavens, A. F., Jimenez, R., 2011, MNRAS, 413, 434
- Toloba, E., Sánchez-Blázquez, P., Gorgas, J., Gibson, B. K., 2009, ApJ, 691, L95
- Trager, S. C., Worthey, G., Faber, S. M., Burstein, D., González, J. J., 1998, ApJS, 116, 1
- Trager, S. C., Faber, S. M., Worthey, G., González, J. J., 2000, AJ, 119, 1645
- Valdes, F., Gupta, R., Rose, J. A., Singh, H. P., Bell, D. J., 2004, ApJS, 152, 251
- van Dokkum P. G., Brammer, G., 2010, ApJ, 718, L73
- Vazdekis, A., 1999, ApJ, 513, 224
- Vazdekis, A., Arimoto, N., 1999, ApJ, 525, 144
- Vazdekis, A., Casuso, E., Peletier, R. F., Beckman, J. E., 1996, ApJS, 106, 307
- Vazdekis, A., Peletier, R. F., Beckman, J. E., Casuso, E., 1997, ApJS, 111, 203
- Vazdekis, A., Cenarro, A. J., Gorgas, J., Cardiel, N., Peletier, R. F., 2003, MNRAS, 340, 1317
- Vazdekis, A., Trujillo, I., Yamada, Y., 2004, ApJ, 601, L33
- Vazdekis, A., Sánchez-Blázquez P., Falcón-Barroso J., Cenarro A. J., Beasley M. A., Cardiel N., Gorgas J., Peletier R. F., 2010, MNRAS, 404, 1639 (Paper I)
- Vazdekis, A., Ricciardelli, E., Cenarro, A. J., Rivero-González, J. G., Díaz-García, L. A., Falcón-Barroso, J., 2012, MNRAS, 424, 157
- Vazdekis, A., Coelho, P., Cassisi, S., Ricciardelli, E., Falcón-Barroso, J., Sánchez-Blázquez, P., La Barbera, F., Beasley, M., Pietrinferni, A., 2015, MNRAS, 449, 1177
- Vázquez, G. A., Leitherer, C., Meynet, G., Maeder, A., 2007, ApJ, 663, 1020
- Walcher, C. J., Coelho, P., Gallazzi, A., Charlot, S., 2009, MNRAS, 398, L44
- Worthey, G., 1994, ApJS, 95, 107
- Worthey, G., Faber, S. M., Gonzalez, J. J., Burstein, D., 1994, ApJS, 94, 687
- Worthey, G., 2004, AJ, 128, 2826
- Worthey, G., Faber, S. M., González, J. J., 1992, ApJ, 398, 69
- Worthey, G., Baitian, T., Serven, J., 2014, ApJ, 783, 20
- Wu, C.-C., Ake, T. B., Boggess, A., et al. 1983, NASA IUE Newsl. (Special ed.), 24, 223
- Yamada, Y., Arimoto, N., Vazdekis, A., Peletier, R. F., 2006, ApJ, 637, 200
- Yi, S. K., Lee, J., Sheen, Y.-K., Jeong, H., Suh, H., Oh, K., 2011, ApJS, 195, 22